Best Theory Diagrams for multilayered plates considering multifield analysis

Best Theory Diagrams for multilayered plates considering multifield analysis

Cinefra M.[1*], Carrera E.[1†], Lamberti A.[1‡], Petrolo M.[2§]

(1) Department of Mechanical and Aerospace Engineering, Politecnico di Torino, 10129 Torino, Italy
(2) School of Aerospace, Mechanical and Manufacturing Engineering, RMIT University,
PO Box 71, Bundoora VIC 3083, Australia

Submitted to:

Journal of Intelligent Material Systems and Structures

Author for correspondence:

M. Cinefra, PhD,
Department of Mechanical and Aerospace Engineering,
Politecnico di Torino,
Corso Duca degli Abruzzi 24,
10129 Torino, Italy,
tel: +39 011 090 6869,
fax: +39 011 090 6899,
e-mail: maria.cinefra@polito.it,
website: www.mul2.com

[*] Department of Mechanical and Aerospace Engineering,, e-mail: maria.cinefra@polito.it
[†] Professor of Aerospace Structures and Aeroelasticity, e-mail: erasmo.carrera@polito.it
[‡] PhD student, e-mail: alessandro.lamberti@polito.it
[§] Research Fellow, SAMME, RMIT, Melbourne, e-mail: marco.petrolo@rmit.edu.au

Abstract

This work presents the Best Theory Diagrams (BTDs) for multilayered plates involved in multifield problems (mechanical, thermal and electrical). A BTD is a curve that reports the minimum number of terms of a refined model for a given accuracy. The Axiomatic/Asymptotic technique is employed in order to detect the relevant terms, and the error is computed with respect to an exact or quasi-exact solution. The models that belong to the BTDs are constructed by means of a genetic algorithm and the Carrera Unified Formulation (CUF). This last defines the displacement field as an expansion of the thickness coordinate. The governing equations are obtained in terms of few fundamental nuclei, whose form does not depend on the particular expansion order that is employed. The Navier closed-form solution has been adopted to solve the equilibrium equations. The analyses herein reported are related to plates subjected to multifield loads: mechanical, thermal and electrical. The aim of this study is to evaluate the influence of the type of the load in the definition of the BTDs. In addition, the influence of geometry, material parameters and displacement/stress components are considered. The results suggest that the BTD and the CUF can be considered as tools to evaluate any structural theory against a reference solution. In addition, it has been found that the BTD definition is influenced to a great extent by the type of load.

1 Introduction

A multifield problem arises when a structure is subjected to loads of a different nature, such as thermal, piezoelectric and mechanical loads. A typical example of such a problem can be a space vehicle during the reentry phase: in this case, the vehicle is subjected to a temperature and pressure distribution. The analysis of the blades of a turbine is another example of multifield problem since the blades are subjected to temperature and pressure distributions at the same time. Another interesting example comes from the so-called smart structures. This type of structures have a piezoelectric layer inside, i.e. a layer of a particular material that deforms under the action of a potential distribution, or conversely, it produces a potential distribution when deformed. Accurate structural models are required to deal with these problems. This paper proposes advanced plate models for the multifield analysis of multilayered structures.

A multifield problem for a plate can be solved by employing classical theories, such as the Kirchoff-Love model (Kirchhoff, 1850; Love, 1927), and including the effect induced by the multifield loads. But, the hypotheses on which this model is based (transverse normal and shear strains are negligible) make it not suitable for the analysis of thick and multilayered plates. Improvements of the Kirchoff-Love model can be obtained if at least one of Kirchhoff's hypotheses are removed. For example, a constant through-the-thickness transverse shear deformation can be taken into consideration. This is the case of the Reissner-Mindlin theory (Reissner, 1945; Mindlin, 1951), also known as the First-order Shear Deformation Theory (FSDT). Further improvements have been introduced in Vlasov's (Vlasov, 1957) or Hildebrand-Reissner-Thomas's theories (Hildebrand et al., 1938), which are based on higher-order expansions of the displacement components on the reference surface. In general, it is possible to affirm that the less restrictive hypotheses are assumed, the more accurate the analysis is. The accuracy of a plate model is also the topic analyzed in Carrera (1997). In that work, the author observed that an accurate plate model should include the C_z^0-requirements, i.e. the transverse stress continuity at the interfaces between the layers (Interlaminar-Continuity (IC)) and the discontinuous distribution along the thickness of the first derivative of the displacement components (this is defined as the Zig-Zag effect (ZZ)). In the history of the structural models, Lekhnitskii (Lekhnitskii, 1968) has first presented a Zig-Zag solution in 1935 for the analysis of multilayered beams.

The C_z^0 requirements are an important feature to account for in the development of an accurate plate model. In addition, another important distinction has to be considered in the field of multilayer plate analysis. A multilayered plate model can be developed considering two types of schemes: the Equivalent Single Layer (ESL) or the Layer Wise (LW) schemes. According to the ESL scheme, the number of the unknowns are not affected by the number of layers, while, in the LW scheme, each layer of the plate has its displacement unknowns. In this case, the number of unknowns of the model is strictly related with the number of layers of the plate. An in-depth discussion on ESL and LW models is reported in the book Reddy (1997).

The analysis of the stress state due to a temperature distribution is pertinent to the thermoelasticity, which is a branch of the applied mechanics. A historical introduction to the thermoelasticity is reported in Hetnarski and Eslami (2009), where the authors describe the J.M.C. Duhamel's work (Duhamel, 1837), Navier and Fourier's (Navier, 1827; Fourier, 1822), Neumann's (Neumann, 1885), Almansi's (Almansi, 1897), Tedone's (Tedone, 1906) and Voigt's (Voigt, 1910). Examples of refined models for thermal stress plate analysis are reported in Tauchert (1991), Noor and Burton (1992) and in Argyris and Tenek (1997). In Tauchert (1991), the author conducted a survey on the response of flat plates to thermal loadings. Isotropic homogeneous, as well as anisotropic or heterogeneous, plates were considered. The author in Noor and Burton (1992) focused on the hierarchy of composite models, predictor-corrector procedures, the effect of the temperature-dependence of the material properties on the response, and the sensitivity of the thermo-mechanical response to variations in the material parameters. The work presented in Argyris and Tenek (1997) describes the developments of the nonlinear thermo-structural analysis of laminated composite plates and shells of arbitrary geometry. Another note that should be considered, whenever one intends to develop a structural model that is able to describe the thermo-mechanical response of a multilayered plate, is by Murakami, which is reported in Murakami (1993).

Piezoelectric materials can be employed to create particular types of plates. The piezoelectric phenomenon was discovered in 1880-1881 by Curie brothers (Jacques and Pierre Curie) for some kinds of natural crystals. This effect can be divided into direct and inverse effect. The former means the generation of a distribution of charge when the piezoelectric material is subjected to a pressure load. The

latter, instead, means the deformation of the piezoelectric material when an electric charge is applied to it. Piezoelectricity can be used to create embedded sensors and embedded actuators. The main advantage offered by these configurations is that a structural health monitoring is possible. A number of mathematical models for piezo-mechanic analysis are available in the scientific literature. In the field of ESL models, classical formulations can be used for piezo-mechanic analysis: an example can be found in Tiersten (1969) and in Mindlin (1972). Another example of refined theory available in the literature is the model proposed in Yang and Yu (1993) by Yang and Yu. A refined model based on the LW approach is presented by Mitchell and Reddy in Mitchell and Reddy (1995): the description of the electric potential is based on a LW approach, while the displacement field of the plate is described by means of an ESL approach.

Among all the refined theories reported in the scientific literature, the Carrera Unified Formulation (CUF) has to be mentioned. The CUF permits the analysis of plates and shells to be performed in a unified manner: the governing equations are derived in terms of few fundamental nuclei whose expressions do not change by varying the assumptions made for the displacement variables in the thickness direction. The analysis of plates and shells under the action of a pressure distribution is reported in Carrera (2003) and Carrera et al. (2014). In addition, in that work the author employs the CUF in the framework of different variational principles. Examples of thermal stress plate analysis conducted by means of the CUF can be found in Carrera (2002), where the author presented an innovative way of computing the internal temperature distribution of a plate. It was demonstrated that the assumption of a linear temperature distribution is no longer valid for thick plates. The use of the CUF for piezo-mechanic analysis can be found in Ballhause et al. (2005). The authors compare the results obtained by means of the CUF with the results reported in the open literature. The CUF is employed, in this work, to obtain the governing equations of multilayered plates for multifield problems.

In all the analyses reported, it is demonstrated that accurate plate analyses can be achieved if higher-order models are employed. The main disadvantage of this strategy is that high computational cost is required. It could be interesting to decrease this cost without loosing in accuracy. This problem was already analyzed in the works Carrera and Petrolo (2010) and Carrera et al. (2011b,c), where refined plate models were considered, and some reduced refined models were presented. That work was based on the axiomatic/asymptotic technique which computes the relevance of the terms of a refined model with respect to a reference solution and discards the terms that do not contribute to the plate analysis. Only ESL models were considered, and it was demonstrated that several parameters affect the relevance of the terms. In particular, the results showed that the geometry (through the length-to-thickness ratio, a/h) and the ortothropic ratio (E_L/E_T) influence the order and the number of the retained terms. Other relevant works on the axiomatic/asymptotic technique are presented in Petrolo and Lamberti (2016) and Mashat et al. (2013), where the authors applied the axiomatic/asymptotic technique to LW models for multilayered plates. The paper Mashat et al. (2014) presents the extension of the axiomatic/asymptotic technique to sandwich shells.

The present work is devoted to the analysis through the axiomatic/asymptotic technique of refined mechanical, thermal and piezoelectric plate theories. The differential equations are obtained by applying the Principle of Virtual Displacements. Both ESL and LW schemes are considered. The governing equations are solved considering the Navier closed-form solution. The purpose of this work is to offer the Best Theory Diagram (BTD) for multifield problems for plates. This particular graph puts into relation the number of terms of a model and its accuracy with respect to a reference solution. The models reported in the BTD have the lowest possible error. The possibility to obtain this graph comes from the use of the axiomatic/asymptotic technique. It should be mentioned that these models are constructed by employing a genetic algorithm, which makes it possible to detect the best terms combinations. Examples of BTDs can be found in Carrera and Miglioretti (2012), where the authors employ a genetic-like algorithm in order to evaluate the BTD for plates under mechanical loads. In addition, the axiomatic/asymptotic technique was employed for the analysis of refined beam theory as reported in Carrera and Petrolo (2011) and Carrera et al. (2012). In this study, the effect of the geometry and the type of the load on the selection of the terms is analyzed.

The present paper is organized as follows: in Section 2 the constitutive relations and the governing equations are described and in Section 3 a brief introduction to plate theory analysis is carried out. The Navier-type closed-form solution is introduced in Section 4 and the governing equations are derived in Section 5. In Section 6, the axiomatic / asymptotic technique and the Best Theory Diagram are presented; the results are reported in Section 7. The conclusions are presented in Section 8.

2 Constitutive equations and variational statements for multi-field problems

The strain-displacement relations for a plate are introduced

$$\boldsymbol{\epsilon}^k = \mathbf{D}\mathbf{u}^k \tag{1}$$

where $\boldsymbol{\epsilon}^k = \left[\epsilon^k_{xx}\ \epsilon^k_{yy}\ \epsilon^k_{zz}\ \epsilon^k_{xy}\ \epsilon^k_{xz}\ \epsilon^k_{yz}\right]^T$ is the vector of the strains of the layer k; $\mathbf{u}^k = \left[u^k_x\ u^k_y\ u^k_z\right]^T$ is the displacement vector; and $\mathbf{D}$ is a differential operator whose components are

$$\mathbf{D} = \begin{bmatrix} \frac{\partial}{\partial x} & 0 & 0 \\ 0 & \frac{\partial}{\partial y} & 0 \\ 0 & 0 & \frac{\partial}{\partial z} \\ \frac{\partial}{\partial y} & \frac{\partial}{\partial x} & 0 \\ \frac{\partial}{\partial z} & 0 & \frac{\partial}{\partial x} \\ 0 & \frac{\partial}{\partial z} & \frac{\partial}{\partial y} \end{bmatrix} \tag{2}$$

These relations are valid for all the analyses reported in the following. It should be mentioned that the strain components can be grouped into in-plane (p) and out-of-plane (n) components, that is

$$\boldsymbol{\epsilon}^k_p = \left[\epsilon^k_{xx}\ \epsilon^k_{yy}\ \epsilon^k_{xy}\right]^T \qquad \boldsymbol{\epsilon}^k_n = \left[\epsilon^k_{xz}\ \epsilon^k_{yz}\ \epsilon^k_{zz}\right]^T \tag{3}$$

The upper script T denotes the transpose operation. In this case, it is possible to write

$$\boldsymbol{\epsilon}^k_p = \mathbf{D}_p\mathbf{u}^k \qquad \boldsymbol{\epsilon}^k_n = \mathbf{D}_n\mathbf{u}^k \tag{4}$$

defining

$$\mathbf{D}_p = \begin{bmatrix} \frac{\partial}{\partial x} & 0 & 0 \\ 0 & \frac{\partial}{\partial y} & 0 \\ \frac{\partial}{\partial y} & \frac{\partial}{\partial x} & 0 \end{bmatrix} \tag{5}$$

$$\mathbf{D}_n = \begin{bmatrix} \frac{\partial}{\partial z} & 0 & \frac{\partial}{\partial x} \\ 0 & \frac{\partial}{\partial z} & \frac{\partial}{\partial y} \\ 0 & 0 & \frac{\partial}{\partial z} \end{bmatrix} = \overbrace{\begin{bmatrix} 0 & 0 & \frac{\partial}{\partial x} \\ 0 & 0 & \frac{\partial}{\partial y} \\ 0 & 0 & 0 \end{bmatrix}}^{\mathbf{D}_{n\Omega}} + \overbrace{\begin{bmatrix} \frac{\partial}{\partial z} & 0 & 0 \\ 0 & \frac{\partial}{\partial z} & 0 \\ 0 & 0 & \frac{\partial}{\partial z} \end{bmatrix}}^{\mathbf{D}_{nz}} \tag{6}$$

The constitutive relations and variational statements for each problem are defined in the next sections.

2.1 Pure-mechanical analysis

Stress components for a generic layer k can be obtained by means of the Hooke's law

$$\boldsymbol{\sigma}^k = \mathbf{C}^k\boldsymbol{\epsilon}^k \tag{7}$$

The elastic coefficients of the matrix $\mathbf{C}$ are expressed in the problem reference system (i.e (x, y, z) system reported in Fig.1). The dependence of the elastic coefficients C_{ij} on Young's modulus, Poisson's ratio, the shear modulus and the fiber angle is not reported. A detailed discussion is reported in the book by Reddy (Reddy, 1997). The stress components can be grouped into in-plane (p) and out-of-plane (n) components as the strain components, i.e.

$$\boldsymbol{\sigma}^k_p = \left[\sigma^k_{xx}\ \sigma^k_{yy}\ \sigma^k_{xy}\right]^T \qquad \boldsymbol{\sigma}^k_n = \left[\sigma^k_{xz}\ \sigma^k_{yz}\ \sigma^k_{zz}\right]^T \tag{8}$$

In this case, the Hooke's law can be defined as

$$\begin{aligned}\boldsymbol{\sigma}_p^k =& \mathbf{C}_{pp}\boldsymbol{\epsilon}_p^k + \mathbf{C}_{pn}\boldsymbol{\epsilon}_n^k \\ \boldsymbol{\sigma}_n^k =& \mathbf{C}_{np}\boldsymbol{\epsilon}_p^k + \mathbf{C}_{nn}\boldsymbol{\epsilon}_n^k\end{aligned} \tag{9}$$

In the case of anisotropic materials it is possible to write

$$\mathbf{C}_{pp}^k = \begin{bmatrix} C_{11}^k & C_{12}^k & C_{16}^k \\ C_{12}^k & C_{22}^k & C_{26}^k \\ C_{16}^k & C_{26}^k & C_{66}^k \end{bmatrix} \qquad \mathbf{C}_{nn}^k = \begin{bmatrix} C_{55}^k & C_{45}^k & 0 \\ C_{45}^k & C_{44}^k & 0 \\ 0 & 0 & C_{33}^k \end{bmatrix} \qquad \mathbf{C}_{pn}^k = \mathbf{C}_{np}^{k^T} = \begin{bmatrix} 0 & 0 & C_{13}^k \\ 0 & 0 & C_{23}^k \\ 0 & 0 & C_{36}^k \end{bmatrix} \tag{10}$$

The analysis of a plate can be conducted by means of the Principle of Virtual Displacements (PVD), that states

$$\sum_{k=1}^{N_L} \delta\, L_{int}^k = \sum_{k=1}^{N_L} \delta\, L_{ext}^k \tag{11}$$

δ denotes the virtual variation. δL_{int}^k is the virtual variation of the strain energy that is computed considering the internal stresses and strain distributions for a generic k layer. δL_{ext}^k is the virtual variation of the work made by the external loadings on the generic layer k. N_L is the total number of layers of a multilayered plate.

In the case of pure-mechanical analysis, the virtual variation of the strain energy can be computed as

$$\delta\, L_{int}^k = \sum_{k=1}^{N_L} \int_{V_k} \left(\delta\boldsymbol{\epsilon}_p^k \cdot \boldsymbol{\sigma}_p^k + \delta\boldsymbol{\epsilon}_n^k \cdot \boldsymbol{\sigma}_n^k\right) dV_k = \sum_{k=1}^{N_L} \int_{\Omega_k} \int_{A_k} \left(\delta\boldsymbol{\epsilon}_p^k \cdot \boldsymbol{\sigma}_p^k + \delta\boldsymbol{\epsilon}_n^k \cdot \boldsymbol{\sigma}_n^k\right) d\Omega_k\, dz_k \tag{12}$$

where V_k is the volume of the layer k. The virtual variation of the external loading can be computed as

$$\delta L_{ext}^k = \sum_{k=1}^{N_L} \int_{V_k} \delta\mathbf{u}^{T^k}\ \mathbf{p}^k\, dV_k \tag{13}$$

$\delta\mathbf{u}^k$ is the virtual variation of the displacement vector $\mathbf{u}^k$ and the components of the vector $\mathbf{p}^k$ are the load distributions according to the reference system axes x, y and z. The operator $\int_{A_k} dz_k$ denotes the integration along the thickness direction. Ω_k is the reference surface of the generic k layer (see Fig. 1).

2.2 Thermal stress analysis

In this work, the uncoupled thermo-mechanical analysis is performed in which the temperature is considered as an external load. A plate subjected to a temperature distribution can be analyzed by defining the thermal stresses as

$$\begin{aligned}\boldsymbol{\sigma}_{pT}^k &= \mathbf{C}_{pp}^k \cdot \boldsymbol{\epsilon}_{pT}^k + \mathbf{C}_{pn}^k \cdot \boldsymbol{\epsilon}_{nT}^k \\ \boldsymbol{\sigma}_{nT}^k &= \mathbf{C}_{pn}^k \cdot \boldsymbol{\epsilon}_{pT}^k + \mathbf{C}_{nn}^k \cdot \boldsymbol{\epsilon}_{nT}^k\end{aligned} \tag{14}$$

where ϵ_{pT} and ϵ_{nT} indicate the in-plane (p) and out-of-plane (n) strains due to a temperature gradient, that is

$$\boldsymbol{\epsilon}_{pT}^k = \begin{bmatrix}\epsilon_{xxT}^k\ \epsilon_{yyT}^k\ \epsilon_{xyT}^k\end{bmatrix} \qquad \boldsymbol{\epsilon}_{nT}^k = \begin{bmatrix}\epsilon_{xzT}^k\ \epsilon_{yzT}^k\ \epsilon_{zzT}^k\end{bmatrix} \tag{15}$$

Considering the thermal expansion coefficient vector α, it is possible to write

$$\begin{aligned}\boldsymbol{\epsilon}_{pT}^k &= \left\{\alpha_1^k,\ \alpha_2^k,\ 0\right\} \cdot \theta^k(x,y,z) = \boldsymbol{\alpha}_p^k \cdot \theta^k(x,y,z) \\ \boldsymbol{\epsilon}_{nT}^k &= \left\{0,\quad 0,\quad \alpha_3^k\right\} \cdot \theta^k(x,y,z) = \boldsymbol{\alpha}_n^k \cdot \theta^k(x,y,z)\end{aligned} \tag{16}$$

where $\theta^k(x,y,z)$ is the relative temperature distribution in a generic k layer referred to a reference temperature θ_e. The subscript 1 denotes the longitudinal direction of the fibers, while 2 and 3 denote the transverse directions to the fibers. Let us recall the PVD in Eq.(11), that is

$$\sum_{k=1}^{N_l} \int_{\Omega_k} \int_{A_k} \left(\delta \boldsymbol{\epsilon}_p^{k^T} \boldsymbol{\sigma}_p^k + \delta \boldsymbol{\epsilon}_n^{k^T} \boldsymbol{\sigma}_n^k \right) dz_k \, d\Omega_k = \delta \, L_{ext} \tag{17}$$

In Eq.(17), stresses $\boldsymbol{\sigma}_p$ and $\boldsymbol{\sigma}_n$ are considered as the sum of the mechanical (H) and thermal (T) contributions, i.e.

$$\begin{aligned} \boldsymbol{\sigma}_p &= \boldsymbol{\sigma}_{pH}^k - \boldsymbol{\sigma}_{pT}^k \\ \boldsymbol{\sigma}_n &= \boldsymbol{\sigma}_{nH}^k - \boldsymbol{\sigma}_{nT}^k \end{aligned} \tag{18}$$

Therefore, the variational statement in (17) can be expressed as

$$\sum_{k=1}^{N_l} \int_{\Omega_k} \int_{A_k} \delta \boldsymbol{\epsilon}_p^{k^T} \left(\boldsymbol{\sigma}_{pH}^k - \boldsymbol{\sigma}_{pT}^k \right) + \delta \boldsymbol{\epsilon}_n^{k^T} \left(\boldsymbol{\sigma}_{nH}^k - \boldsymbol{\sigma}_{nT}^k \right) \, dz_k \, d\Omega_k = \sum_{k=1}^{N_L} \delta \, L_{ext}^k \tag{19}$$

2.3 Piezo/mechanical analysis

Direct and converse piezoelectric effects define the coupling effect between stresses and electric field. The constitutive equations for piezoelectric materials are defined according to the IEEE standard (A.N.S. Institute, 1987) and are

$$\begin{aligned} \boldsymbol{\sigma}^k &= \mathbf{C}^k \boldsymbol{\epsilon}^k - \mathbf{e}^{k^T} \mathbf{E}^k \\ \tilde{\mathbf{D}}^k &= \mathbf{e}^k \boldsymbol{\epsilon}^k + \boldsymbol{\varepsilon}^k \mathbf{E}^k \end{aligned} \tag{20}$$

where $\tilde{\mathbf{D}}^k$ is the dielectric displacement and $\mathbf{E}^k$ is the electric field

$$\tilde{\mathbf{D}}^k = \left[\tilde{D}_1^k, \tilde{D}_2^k, \tilde{D}_3^k \right]^T \qquad \mathbf{E}^k = \left[E_1^k, E_2^k, E_3^k \right]^T \tag{21}$$

$\mathbf{e}^k$ is the matrix of the piezoelectric constants:

$$\mathbf{e}^k = \begin{bmatrix} 0 & 0 & 0 & e_{14}^k & e_{15}^k & 0 \\ 0 & 0 & 0 & e_{24}^k & e_{25}^k & 0 \\ e_{31}^k & e_{32}^k & e_{36}^k & 0 & 0 & e_{33}^k \end{bmatrix} \tag{22}$$

and $\boldsymbol{\varepsilon}^k$ is the matrix of the permittivity coefficients of the k-layer

$$\boldsymbol{\varepsilon}^k = \begin{bmatrix} \varepsilon_{11}^k & \varepsilon_{12}^k & 0 \\ \varepsilon_{21}^k & \varepsilon_{22}^k & 0 \\ 0 & 0 & \varepsilon_{33}^k \end{bmatrix} \tag{23}$$

In the following only hexagonal crystal systems are considered, this implies that $\varepsilon_{12} = \varepsilon_{21} = 0$ (A.N.S. Institute, 1987).

The piezo-mechanic equations can be written dividing the stress and deformation components into in-plane (p) and out-of-plane (n) components for a generic k layer. In this case, it is possible to write

$$\begin{aligned} \boldsymbol{\sigma}_p^k &= \mathbf{C}_{pp} \boldsymbol{\epsilon}_{pp}^k + \mathbf{C}_{pn} \boldsymbol{\epsilon}_{pn}^k - \mathbf{e}_p^{k^T} \mathbf{E}^k \\ \boldsymbol{\sigma}_n^k &= \mathbf{C}_{pn}^T \boldsymbol{\epsilon}_{pp}^k + \mathbf{C}_{nn} \boldsymbol{\epsilon}_{pn}^k - \mathbf{e}_n^{k^T} \mathbf{E}^k \\ \tilde{\mathbf{D}}^k &= \mathbf{e}_p^k \boldsymbol{\epsilon}_p^k + \mathbf{e}_n^k \boldsymbol{\epsilon}_n^k + \boldsymbol{\varepsilon}^k \mathbf{E}^k \end{aligned} \tag{24}$$

where

$$\mathbf{e}_p^k = \begin{bmatrix} 0 & 0 & 0 \\ 0 & 0 & 0 \\ e_{31}^k & e_{32}^k & e_{36}^k \end{bmatrix} \quad \mathbf{e}_n^k = \begin{bmatrix} e_{14}^k & e_{15}^k & 0 \\ e_{24}^k & e_{25}^k & 0 \\ 0 & 0 & e_{33}^k \end{bmatrix} \tag{25}$$

The electric field $\mathbf{E}^k$ can be derived from the Maxwell equations

$$\mathbf{E}^k = \mathbf{D}_e \Phi^k \tag{26}$$

where

$$\mathbf{D}_e = \begin{bmatrix} -\partial_{,x} & 0 & 0 \\ 0 & -\partial_{,y} & 0 \\ 0 & 0 & -\partial_{,z} \end{bmatrix} \tag{27}$$

and Φ^k is the electric potential. In this work, two configurations are considered: sensor and actuator. Sensor configuration means that a piezoelectric plate is subjected only to external mechanical loadings, and the resulting deformation state causes the potential distribution. Actuator configuration means that the deformation of the piezoelectric plate is caused by the piezoelectric layers as a consequence of the application of a potential distribution. Both configurations are reported in Fig. 2. Further details can be found in Ballhause et al. (2005) and in Carrera et al. (2011).

The potential distribution is a scalar quantity, but for implementation reasons it is convenient to define it as a vector, i.e. $\mathbf{\Phi}^k = \begin{bmatrix} \Phi^k & \Phi^k & \Phi^k \end{bmatrix}^T$. In this case, the matrix of differential operators can be expressed as

$$\mathbf{D}_e = \begin{bmatrix} -\partial_{,x} & 0 & 0 \\ 0 & -\partial_{,y} & 0 \\ 0 & 0 & -\partial_{,z} \end{bmatrix} = \underbrace{\begin{bmatrix} -\partial_{,x} & 0 & 0 \\ 0 & -\partial_{,y} & 0 \\ 0 & 0 & 0 \end{bmatrix}}_{\mathbf{D}_{e\Omega}} + \underbrace{\begin{bmatrix} 0 & 0 & 0 \\ 0 & 0 & 0 \\ 0 & 0 & -\partial_{,z} \end{bmatrix}}_{\mathbf{D}_{ez}} \tag{28}$$

The analysis of a piezoelectric plate can be conducted by means of the Principle of Virtual Displacement (PVD) (see Eq.(11)) extended to the electro-mechanical problem, that states

$$\sum_{k=1}^{N_L} \int_{V_k} \left(\delta \boldsymbol{\epsilon}_p^{k^T} \cdot \boldsymbol{\sigma}_p^k + \delta \boldsymbol{\epsilon}_n^{k^T} \cdot \boldsymbol{\sigma}_n^k - \delta \mathbf{E}^{k^T} \, \tilde{\mathbf{D}}^k \right) dV_k = \sum_{k=1}^{N_L} \delta \, L_{ext}^k \tag{29}$$

3 Considered plate theories

Plate geometry is reported in Fig. 1, the reference surface is denoted as Ω and its boundary as Γ. The reference system axes which belong to the reference surface Ω are denoted as x, y, and z is the thickness coordinate. The length side dimensions of the plate are indicated as a and b, and the thickness of the plate is defined as h.

In the framework of the Carrera Unified Formulation, the displacement field of a plate can be described as:

$$\mathbf{u}(x, y, z) = F_\tau(z) \cdot \mathbf{u}_\tau(x, y) \qquad \tau = 1, 2, \ldots, N+1 \tag{30}$$

where a summation on the index τ is implied according to the Einstein notation. $\mathbf{u}$ is the displacement vector $(u_x \; u_y \; u_z)$, whose components are the displacements along the x, y, z reference axes, (see Fig. 1). F_τ are the so-called thickness functions depending on z and $\mathbf{u}_\tau = (u_{\tau x}, \; u_{\tau y}, \; u_{\tau z})$ are the displacement variables depending on the in-plane coordinates x, y; N is the order of expansion.

The expansion functions F_τ can be defined on the overall thickness of the plate or for each k-layer. In the former case Equivalent Single Layer (ESL) approach is followed, while, in the latter case, a Layer Wise (LW) approach is used. Examples of ESL and LW schemes are reported in Fig.s 3(a) and 3(b), respectively: a transverse section of a multilayered plate is reported, the number of layers is equal to N_L. A generic displacement component distribution is presented according to linear and higher order expansion for both approaches. For the ESL case, the location of the point P on the total thickness is z_P (Fig. 3(a)), while for LW scheme the point P is defined according to the local k-layer reference system labeled in the figure as x_k, y_k, ζ_k (Fig. 3(b)). In the following, ESL and LW approaches are discussed in detail.

3.1 Equivalent Single Layer theory

According to the ESL scheme, a multilayered plate is analyzed as a single equivalent lamina. In this case, the F_τ functions can be Mc-Laurin expansions of z, defined as $F_\tau = z^{\tau-1}$. In the following, the ESL models are indicated as EDN, where N is the expansion order. An example of an ED4 displacement field is reported

$$\begin{aligned} u_x &= u_{x_1} + z\,u_{x_2} + z^2\,u_{x_3} + z^3\,u_{x_4} + z^4\,u_{x_5} \\ u_y &= u_{y_1} + z\,u_{y_2} + z^2\,u_{y_3} + z^3\,u_{y_4} + z^4\,u_{y_5} \\ u_z &= u_{z_1} + z\,u_{z_2} + z^2\,u_{z_3} + z^3\,u_{z_4} + z^4\,u_{z_5} \end{aligned} \tag{31}$$

It should be mentioned that, in the case of ED1 models (and in general, in the case of all ESL models), whenever only a constant or a linear expansion is considered for the u_z displacement component, the thickness locking correction should be applied. The first order models based on the ESL scheme present the so-called *thickness locking* (TL), i.e. the simplified kinematic assumptions in the plate analysis do not permit the 3D solution to be reached when thin plates are analyzed. In Carrera and Brischetto (2008), the authors analyze and propose some solutions for this problem.

3.2 Layer Wise theory

According to the Layer Wise scheme, the displacement field exhibits only C_0-continuity through the laminate thickness. LW models can be conveniently built by using a Legendre's polynomials expansion in each layer. The displacement field is described as

$$\mathbf{u}^k = F_t \cdot \mathbf{u}_t^k + F_b \cdot \mathbf{u}_b^k + F_r \cdot \mathbf{u}_r^k = F_\tau \mathbf{u}_\tau^k \qquad \tau = t, b, r \;\; r = 2, 3, \ldots, N \qquad k = 1, 2, \ldots, N_l \tag{32}$$

where k indicates the generic k-layer of the plate and N_l is the number of the layers. Subscripts t and b correspond to the top and bottom surfaces of the layer. Functions F_τ depend on the coordinate ζ_k and its range is $-1 \leq \zeta_k \leq 1$; its representation is reported in Fig. 3(b). The functions F_τ are linear combinations of the Legendre's polynomials according to the following equations:

$$F_t = \frac{P_0 + P_1}{2} \qquad F_b = \frac{P_0 - P_1}{2} \qquad F_r = P_r - P_{r-2} \qquad r = 2, 3, \ldots, N \tag{33}$$

The Legendre's polynomials up to the fourth order are:

$$P_0 = 1 \quad P_1 = \zeta_k \quad P_2 = \frac{3\zeta_k^2 - 1}{2} \quad P_3 = \frac{5\zeta_k^3 - 3\zeta_k}{2} \quad P_4 = \frac{35\zeta_k^4}{8} - \frac{15\zeta_k^2}{4} + \frac{3}{8} \tag{34}$$

LW models ensure the compatibility of the displacement at the interfaces and the 'zig-zag' effects by definition, that is

$$\mathbf{u}_t^k = \mathbf{u}_b^{k+1} \qquad k = 1, \ldots, N_l - 1 \tag{35}$$

In the following, the LW models are denoted by the acronym as LDN, where N is the expansion order. An example of LD4 layer displacement field is

$$\begin{aligned} u_x^k &= F_t\,u_{xt}^k + F_2\,u_{x2}^k + F_3\,u_{x3}^k + F_4\,u_{x4}^k + F_b\,u_{xb}^k \\ u_y^k &= F_t\,u_{yt}^k + F_2\,u_{y2}^k + F_3\,u_{y3}^k + F_4\,u_{y4}^k + F_b\,u_{yb}^k \\ u_z^k &= F_t\,u_{zt}^k + F_2\,u_{z2}^k + F_3\,u_{z3}^k + F_4\,u_{z4}^k + F_b\,u_{zb}^k \end{aligned} \tag{36}$$

More details about the CUF can be found in the Carrera's works (Carrera, 2003; Carrera et al., 2010, 2011,a, 2014).
In general a temperature distribution for a generic k layer can be conveniently described by means of an LW approach, that is

$$\theta^k(x, y, z) = F_t \cdot \theta_t^k(x, y) + F_r \cdot \theta_r^k(x, y) + F_b \cdot \theta_b^k(x, y) = F_\tau \theta_\tau^k(x, y) \tag{37}$$

Functions θ_τ^k are defined as

$$\theta_\tau^k = \overline{\theta}_\tau^k - \theta_e \tag{38}$$

where $\overline{\theta}_\tau^k$ is the effective temperature distribution. The temperature distribution can be defined by solving the conduction equation for a given temperature distribution over the lateral, top and bottom surfaces. The approach proposed in Eq.(37) offers the possibility to impose the continuity of the temperature distribution along the thickness direction. In Carrera (2002) further details on the temperature distribution evaluation can be found. However, a simple linear temperature distribution is here considered for the numerical investigations. A representation of the assumed linear temperature distribution θ_z is reported in Fig. 4 and it is defined as

$$\theta_z = \theta_z^0 \frac{2\,z}{h} + \overline{\theta}_0 \tag{39}$$

h is the total thickness of the plate and the parameters θ_z^0 and $\overline{\theta}_0$ have to be defined according to the desired top and bottom temperature values.
Regarding the electro-mechanical problem, the layers of the multilayered plates herein considered can be piezoelectric or pure elastic. In this case, the differences of the electric properties of each layer can be significant. In the following, the electric potential distribution is expressed according to an LW form distribution since an ESL scheme seems to not be appropriate when non-piezo layers are included in the structure. The potential distribution is then defined as:

$$\Phi = F_t\Phi_t + F_r\Phi_r + F_b\Phi_b = F_\tau\Phi_\tau \qquad \tau = t, r, b \; r = 2, 3, 4 \tag{40}$$

The continuity of the potential distribution at the layers interfaces has to be imposed:

$$\Phi_t^k = \Phi_b^{k+1} \qquad k = 1, \cdots, N_L - 1 \tag{41}$$

where N_L is the number of layers. The expansion order of the potential distribution is assumed to be equal to the expansion order of the displacement field, independently from the adopted scheme (ESL or LW).

4 Navier-type close-form solution

The attention has been here restricted to the case of closed form solutions related to simply supported, cross-ply orthotropic rectangular plates ($C_{16} = C_{26} = C_{36} = C_{45} = 0$) loaded by a harmonic distribution of transverse loadings. The displacement components are therefore expressed in the following harmonic form:

$$\begin{aligned} u_{x_\tau}^k &= \hat{U}_{x_\tau}^k \cdot \cos\left(\tfrac{m\pi x_k}{a_k}\right) \sin\left(\tfrac{n\pi y_k}{b_k}\right) \\ u_{y_\tau}^k &= \hat{U}_{y_\tau}^k \cdot \sin\left(\tfrac{m\pi x_k}{a_k}\right) \cos\left(\tfrac{n\pi y_k}{b_k}\right) \\ u_{z_\tau}^k &= \hat{U}_{z_\tau}^k \cdot \sin\left(\tfrac{m\pi x_k}{a_k}\right) \sin\left(\tfrac{n\pi y_k}{b_k}\right) \end{aligned} \qquad \begin{aligned} &k = 1, N_L \\ &\tau = 0, N \end{aligned} \tag{42}$$

where $\hat{U}_{x_\tau}^k$, $\hat{U}_{y_\tau}^k$, $\hat{U}_{z_\tau}^k$ are the amplitudes, m and n are the number of half-waves (the range varies from 0 to ∞) and a_k and b_k are the dimensions of the plate. The same solution can be applied to ESL approach and, in this case, the displacement variables appear without the superscript k.
The same assumptions are made for the temperature and the electric potential. Therefore, the in-plane distribution of the temperature is

$$\theta_\tau^k = \hat{\theta}_\tau^k \sin\left(\frac{m\pi x_k}{a_k}\right) \sin\left(\frac{n\pi y_k}{b_k}\right) \tag{43}$$

and, in the case of piezo-mechanical analysis, the potential distribution can be defined as

$$\Phi_\tau^k = \hat{\Phi}_\tau^k \cdot \sin\left(\frac{m\pi x_k}{a_k}\right) \sin\left(\frac{n\pi y_k}{b_k}\right) \tag{44}$$

where $\hat{\theta}_\tau^k$ and $\hat{\Phi}_\tau^k$ are the amplitudes of the temperature and the potential, respectively.

5 Governing equations

The governing equations are obtained substituting the geometrical relations, the constitutive equations for the different problems and the variable assumptions (Unified Formulation and Navier's solution) in the variational statements presented in Section 2. The derivation is herein omitted for the sake of brevity; details can be found in the already mentioned CUF works and books.
Substituting in Eqs. (12) and (13), the governing equations in the case of pure-mechanical analysis can be written as

$$\delta \mathbf{u}_s^{k^T} \; : \; \mathbf{K}_{uu}^{k\tau s} \cdot \mathbf{u}_\tau^k = \mathbf{P}_{u\tau}^\tau \tag{45}$$

and the boundary conditions on edge Γ^k as

$$\delta \mathbf{u}_s^{k^T} \; : \; \mathbf{u}_k^\tau = \overline{\mathbf{u}}_k^\tau \quad \text{or} \quad \mathbf{\Pi}_{uu}^{k\tau s} \mathbf{u}_\tau^k = \mathbf{\Pi}_{uu}^{k\tau s} \overline{\mathbf{u}}_\tau^k \tag{46}$$

that are Dirichlet-type and Neumann-type boundary conditions, respectively. The bar symbol indicates assigned value.
$\mathbf{P}_{u\tau}^\tau$ is the external load. The fundamental nucleus of the stiffness matrix, $\mathbf{K}_{uu}^{\tau s}$, is assembled through the indexes τ and s, which consider the order of the expansion in z for the displacements. $\mathbf{\Pi}_{uu}^{k\tau s}$ is the fundamental nucleus of the boundary conditions deriving from the integration by parts of the PVD. The explicit form of the fundamental nuclei can be found in Carrera (2003). Starting from the variational statement in (19), one obtains the governing equations for the thermo-mechanical problem, that are

$$\delta \mathbf{u}_s^{k^T} \; : \; \mathbf{K}_{uu}^{k\tau s} \mathbf{u}_\tau^k = -\mathbf{K}_{u\theta}^{k\tau s} \theta + \mathbf{p}_{us}^k \tag{47}$$

with the related boundary conditions are

$$\delta \mathbf{u}_s^{k^T} \; : \; \mathbf{u}_k^\tau = \overline{\mathbf{u}}_k^\tau \quad \text{or} \quad \mathbf{\Pi}_{uu}^{k\tau s} \mathbf{u}_\tau^k = \mathbf{\Pi}_{uu}^{k\tau s} \overline{\mathbf{u}}_\tau^k \tag{48}$$

The temperature is considered as an external load and it is assigned. The definition of the fundamental nuclei $\mathbf{K}_{uu}^{k\tau s}$, $\mathbf{K}_{u\theta}^{k\tau s}$ and $\mathbf{\Pi}_{uu}^{k\tau s}$ can be found in Carrera and Brischetto (2010). Finally, using the equation (29), the governing equations calculated for the electro-mechanical problem are:

$$\begin{aligned} \delta \, \mathbf{u}_k^s : \quad & \mathbf{K}_{uu}^{k\tau s} \mathbf{u}_\tau^k + \mathbf{K}_{ue}^{k\tau s} \mathbf{\Phi}_\tau^k = \mathbf{p}_{ms}^k \\ \delta \, \mathbf{\Phi}_k^s : \quad & \mathbf{K}_{eu}^{k\tau s} \mathbf{u}_\tau^k + \mathbf{K}_{ee}^{k\tau s} \mathbf{\Phi}_\tau^k = \mathbf{p}_{es}^k \end{aligned} \tag{49}$$

with the boundary conditions

$$\begin{aligned} \delta \, \mathbf{u}_k^s : \; & \mathbf{u}_k^\tau = \overline{\mathbf{u}}_k^\tau \quad \text{or} \quad \mathbf{\Pi}_{uu}^{k\tau s} \mathbf{u}_\tau^k + \mathbf{\Pi}_{ue}^{k\tau s} \mathbf{\Phi}_\tau^k = \mathbf{\Pi}_{uu}^{k\tau s} \overline{\mathbf{u}}_\tau^k + \mathbf{\Pi}_{ue}^{k\tau s} \overline{\mathbf{\Phi}}_\tau^k \\ \delta \, \mathbf{\Phi}_k^s : \; & \mathbf{\Phi}_k^\tau = \overline{\mathbf{\Phi}}_k^\tau \quad \text{or} \quad \mathbf{\Pi}_{eu}^{k\tau s} \mathbf{u}_\tau^k + \mathbf{\Pi}_{ee}^{k\tau s} \mathbf{\Phi}_\tau^k = \mathbf{\Pi}_{eu}^{k\tau s} \overline{\mathbf{u}}_\tau^k + \mathbf{\Pi}_{ee}^{k\tau s} \overline{\mathbf{\Phi}}_\tau^k \end{aligned} \tag{50}$$

The definition of the fundamental nuclei $\mathbf{K}_{uu}^{k\tau s}$, $\mathbf{K}_{ue}^{k\tau s}$, $\mathbf{K}_{eu}^{k\tau s}$, $\mathbf{K}_{ee}^{k\tau s}$, $\mathbf{\Pi}_{uu}^{k\tau s}$, $\mathbf{\Pi}_{ue}^{k\tau s}$, $\mathbf{\Pi}_{eu}^{k\tau s}$ and $\mathbf{\Pi}_{ee}^{k\tau s}$ can be found in Ballhause et al. (2005).

6 The axiomatic/asymptotic method and the Best Theory Diagram

Accurate plate analyses can be obtained by increasing the order of the expansion. As a drawback, the computational cost could increase significantly with respect to the classical formulations. In some works, as in Carrera and Petrolo (2010), it was highlighted that, for a given problem, some terms of a refined model do not contribute to the evaluation of the behavior of the structure. The axiomatic/asymptotic method was introduced in order to detect the ineffective variables for a given problem. In this case, it is possible to ignore such terms in order to reduce the computational cost without loosing in accuracy. In the following the axiomatic/asymptotic technique is described, the Best Theory Diagram (BTD) is introduced and then a method to construct a BTD is explained.

6.1 Axiomatic/asymptotic technique

The possibility to construct reduced models is offered by the axiomatic/asymptotic technique which consists of the following steps:

1. parameters, such as the geometry, BC, loadings, materials and layer layouts, are fixed;
2. a set of output parameters is chosen, such as displacement or stress components; in the following analyses, σ_{xx} and ϕ are considered;
3. a starting theory is fixed (axiomatic part), that is the displacement field is defined; usually a theory which provides 3D-like solutions is chosen; a reference solution is defined (in the present work LD4 and ED4 approaches are adopted, since these fourth-order models offer an excellent agreement with the three-dimensional solutions as highlighted in Carrera and Petrolo (2010) and in Petrolo and Lamberti (2016));
4. the CUF is used to generate the governing equations for the theories considered;
5. the effectiveness of each term of the adopted expansion is evaluated by measuring the error due to its deactivation; a term is considered as non-effective if its error is below an a-priori defined threshold; the deactivation of a term is obtained by means of a penalty technique;
6. the most suitable structural model for a given structural problem is then obtained discarding the non-effective displacement variables.

A graphical notation is introduced in order to represent the results. It consists of a table with three lines, and a number of columns equal to the number of the displacement variables used in the expansion. For example, if an LD4 model for a two-layers plate is considered, its representation is reported in Tab. 1 and it is defined as "Full model representation". If the terms u^1_{z2} and u^2_{x2} are suppressed, the model obtained is represented in Tab. 1 and it is labeled as "Reduced model representation". The meaning of the symbols reported in Tab. 1 is reported in Tab. 2. Symbol ■ is used to denote the terms that can not be suppressed in the LW approach due to the displacement continuity (Eq.(35)).

6.2 The Best Theory Diagram (BTD)

It is possible to associate to each reduced refined model the number of the active terms and its error computed with respect to a reference solution. This information is susceptible of an interesting graphical representation as reported in Fig. 5. The error values are reported on the abscissa, and the number of active terms is reported on the ordinate. Each black dot represents a reduced refined model and its position on the Cartesian plane is defined considering its error and the number of the active terms. In addition, the representation of the active/non-active terms is reported for some reduced models. Among all the models, it is possible to note that some of them present the lowest error for a given number of active terms. These models are labeled in Fig. 5 as 1, 2, 3, 4, 5, and they represent a Pareto front for the considered problems. This Pareto front is defined in this work as the Best Theory Diagram. The existence of such curve was already demonstrated in the work reported in Carrera and Miglioretti (2012). This curve can be constructed for several problems, for example considering several type of materials, geometries and boundary conditions. Moreover, the information reported in a BTD makes it possible to evaluate the minimum number of terms, N_{min}, that have to be used in order to achieve the desired accuracy.

6.3 BTD construction by means of genetic algorithms

The number of all possible combinations of active/not-active terms for a given refined model is equal to 2^M, where M is the number of terms in the model. In the case of an ESL model, M can be computed as

$$M = (N+1)\,3 \tag{51}$$

In the case of an LW model, the displacement field assumed per each layer must satisfy the continuity condition at the interface, so the number M is computed as

$$M = 3\,(N-1)\;N_L \tag{52}$$

As the expansion order increases, the number of the combinations to consider also increases. In this case, the computational cost required for the BTD construction can be very significant. In order to construct a BTD with a minimal computation effort, a different strategy has to be employed. For this purpose in this work, a genetic approach is used, and its implementation is discussed in the following.

The genetic algorithms are inspired by the evolution theory explained in "The origin of species", written by Darwin (Darwin, 1859). In nature, weak and unfit individuals within their environment are faced with extinction by natural selection. The strong ones have a greater opportunity to pass their genes down to future generations via reproduction. In the long run, the species carrying the correct combination in their genes become dominant in their population. Sometimes, during the slow process of evolution, random changes may occur in the genes. If these changes provide additional advantages within the challenge of survival, new species evolve from the old ones. Unsuccessful changes are eliminated by natural selection. In genetic algorithm terminology, a solution vector $\boldsymbol{x} \in \boldsymbol{X}$, where $\boldsymbol{X}$ is the solution space, is called *individual* or *chromosome*. Individuals are made of discrete units called *genes*. Each gene controls one or more features of the individual. The present genetic algorithm use the *mutation* operator to generate new solutions from existing ones. The mutation operator introduces random changes into the characteristics of the chromosome. Mutation is applied at gene level. In the multi-objective optimization genetic algorithm, each individual has a fitness value based on its rank in the population, not its actual objective function value. The population is ranked according to the dominance rule reported in Fonseca and Fleming (1993). The fitness of each chromosome is evaluated through the following formula:

$$r_i(\boldsymbol{x}_i, t) = 1 + nq(\boldsymbol{x}_i, t) \tag{53}$$

where $nq(\boldsymbol{x}, t)$ is the number of solutions dominating by solution $\boldsymbol{x}$ at generation t. A lower rank corresponds to a better solution.
In the present work, each plate theory has been considered as an individual. The genes are the terms of the expansion, and each gene can be active or not active; the deactivation of a term is obtained by exploiting a penalty technique. A representation of this is reported in Fig. 6. The meaning of the symbols ▲ and △ is reported in Tab. 2. Each individual is, therefore, described by the number of active terms and its error computed with respect to a reference solution. Through these two parameters, it is possible to apply the dominance rule in order to evaluate the individuals fitness. The generation of new refined theories starting from a generic population is inspired to the reproduction of bacteria. For each individual (plate theory) a number of copies are created according to its dominance and then, a number of mutations are applied in order to vary the set of new individuals. The purpose of this analysis is to find the individuals which belong to the Pareto front, that is the subset of individuals which are dominated by no other individuals. In all the cases, the number of generations, i.e. iterations, needed is equal to 10 and the number of the initial population is equal to 400. The error of the reduced models with respect to a reference solution is evaluated through the following formula:

$$e = 100\,\frac{\sum_{i=1}^{N_p} |Q^i - Q^i_{\mathrm{ref}}|}{\max Q_{\mathrm{ref}}} \cdot \frac{1}{N_p} \tag{54}$$

where Q is the entity under exam (stress/displacement component) and N_p is the number of points along the thickness on which the entity Q is computed.

7 Results

Best Theory Diagrams (BTDs) for simply supported multilayered plates are reported in the following. These curves are obtained by considering a pure transverse pressure distribution, a temperature distribution and an electric potential distribution, separately. Both ESL and LW schemes are considered.

The BTDs for the mechanical case are obtained by considering a transverse pressure distribution defined as:

$$p_z = p_z^0\,\sin\left(\frac{m\,\pi}{a}\,x\right)\,\sin\left(\frac{n\,\pi}{b}\,y\right) \qquad \mathrm{m} = \mathrm{n} = 1 \tag{55}$$

The number of the half-waves m and n are equal to 1, and the pressure distribution is applied to the top surface of the plate. The dimensions of the plate are $a = b = 1$ and the total thickness is derived from the ratio a/h. The BTDs for the thermal case are obtained by considering a temperature distribution defined as in the Eq.s(43) and (39). In the cases herein considered, the top and bottom temperatures (t_{top}, t_{bot}) are equal to 1 and -1, respectively.

The BTDs for the piezoelectric case are defined by analyzing two different configurations: the sensor and actuator configurations. In the case of a sensor configuration, a transverse pressure is applied to the top surface of the plate and the potential distribution is evaluated. The potential at the top and bottom is set to zero. In the case of an actuator configuration, a potential distribution is applied to the plate, and the value of the potential is set to 1 V at the top and to 0 V at the bottom. The sensor and actuator configurations will be defined as problem 1 and problem 2, respectively. In the case of sensor configuration, the pressure is assumed as in Eq.(55), while, in the case of actuator, the potential distribution is assumed as

$$\Phi = \overline{\Phi} \sin\left(\frac{m\,\pi}{a}\,x\right) \sin\left(\frac{n\,\pi}{b}\,y\right) \tag{56}$$

where $m = n = 1$. The reference system layout and the representation of the two configurations are reported in Fig. 2. $\overline{\Phi}$ is set equal to 1.

The definition of a BTD is possible if a reference solution is available. The BTDs reported in this work are based on the solution computed by means of the LD4 model that in previous works was demonstrated to be in excellent agreement with the elastic solutions. The interested readers can refer to Carrera (2003) for the mechanical case, to Carrera (2002) for the thermal stress analysis and to Ballhause et al. (2005) for the piezo-mechanic analysis. The results are provided in terms of maximum amplitude of sinusoidal distribution, so the transverse displacement u_z and normal stresses σ_{xx}, σ_{yy} and σ_{zz} are evaluated in the center of the plate $(a/2, b/2)$, the shear stress σ_{xz} in $(a, b/2)$, σ_{yz} in $(a/2, b)$ and σ_{xy} in (a, b).

In this work, assessments for the multifield plate analysis are reported. The assessments of the LD4 model for the mechanical and thermal stress analysis are conducted by considering the results reported in Pagano (1970) and Bhaskar et al. (1996), respectively. In both cases, a multilayered plate is considered and the pressure and temperature distributions are assumed as in Eq.s(55) (mechanical case), (43) and (39) (thermal case). The material properties are $E_L/E_T = 25$, $G_{LT}/E_T = G_{TT}/E_T = 0.5$, $G_{Lz}/E_T = 0.2$, $\nu = 0.25$ and $\alpha_L/\alpha_T = 1125$, where E is the Young's modulus, G the shear modulus, ν the Poisson's ratio and α the coefficient of thermal expansion. L and T are the directions parallel and transverse to the composite fibers, respectively. The ply sequence is $(0°/90°/0°)$ for the 3-layers laminate and $(0°/90°/0°/90°/0°)$ for the 5-layers one. In the 3-layers configuration, the layers have equal thickness. In the 5-layers configuration, the total of the thicknesses of $0°$ layers is equal to that one of $90°$ layers and the layers with same orientation have equal thickness between them. Under these conditions, the effective laminate stiffnesses in the x and y directions are the same (Pagano, 1970). The temperature values at the top and at the bottom of the plate are $t_{top} = 1.0$ and $t_{bot} = -1.0$. The results for the mechanical and thermal cases are reported in Tab.s 3 and 4, respectively. In the case of cylindrical thermal load, the sinus is taken in x direction. The stress σ_{xy} has different values at $z = +h/2$ and $z = -h/2$ for the three layer LD4 $a/h = 4$ case and not for the $a/h = 100$ case because the first one corresponds to thick plate configuration and the asymmetry due to the external load is more pronounced. It is possible to note the excellent agreement of the results offered by the LD4 model with the analytical solutions reported from Pagano (1970) and Bhaskar et al. (1996). The BTDs are obtained by computing the accuracies of the reduced refined models in respect to the solution calculated by means of the LD4 model.

The assessment of LD4 model is carried out for the piezoelectric case with respect the case analyzed in Heyliger (1994). LD4 model assessment considers a two-layers laminated plate with two external piezoelectric layers at the top and bottom. The elastic materials properties of laminated layers are: $E_1 = 132.38 \times 10^9$ Pa, $E_2 = E_3 = 10.756 \times 10^9$ Pa, $G_{12} = G_{13} = 5.6537 \times 10^9$ Pa, $G_{23} = 3.606 \times 10^9$ Pa, $\nu_{12} = \nu_{13} = 0.24$, $\nu_{23} = 0.49$, $\varepsilon_{11} = 3.098966 \times 10^{-11}$ C/Vm, $\varepsilon_{22} = \varepsilon_{33} = 2.6562563 \times 10^{-11}$ C/Vm. The thickness for each of these layers is equal to $h = 0.4 \cdot h_{\mathrm{TOT}}$ and the ply sequence is $(90°/0°)$ from bottom to top of the plate. The piezoelectric layers are made of PZT-4 and their properties are $E_1 = E_2 = 81.3 \times 10^9$ Pa, $E_3 = 64.5 \times 10^9$ Pa, $\nu_{12} = 0.329$, $\nu_{13} = \nu_{23} = 0.432$, $G_{44} = G_{55} = 25.6 \times 10^9$Pa, $G_{66} = 30.6 \times 10^9$Pa, $e_{31} = e_{32} = -5.20\mathrm{C/m}^2$, $e_{33} = 15.08\mathrm{C/m}^2$, $e_{24} = e_{15} = 12.72\mathrm{C/m}^2$, $\varepsilon_{11}/\varepsilon_0 = \varepsilon_{22}/\varepsilon_0 = 1475$, $\varepsilon_{33}/\varepsilon_0 = 1300$ ($\varepsilon_0 = 8.854 \times 10^{-12}$C/Vm). The thickness of these layers is equal to $h = 0.1 \cdot h_{\mathrm{TOT}}$. The results are reported in Tab. 5 (sensor configuration) and in Tab. 6 (actuator configuration). It is possible to note

that the LD4 offers a good agreement with the exact solution and, for this reason, it is used as reference solution for definition of the BTDs for the piezo-mechanic analysis.

The BTDs reported in this work are related to a 4-layers plate. The top and bottom layers are made of PZT-4, of which properties were already introduced for the LD4 model assessment. The thermal expansion coefficients are $\alpha_1 = \alpha_2 = 3.8 \times 10^{-6}\,\mathrm{K}^{-1}$ and $\alpha_3 = 1.7 \times 10^{-6}\,\mathrm{K}^{-1}$. The second and third layers of the plate are made of the same elastic material considered during the assessment, the thermal expansion coefficients are equal to $\alpha_1 = -1. \times 10^{-6}\,\mathrm{K}^{-1}$, and $\alpha_2 = \alpha_3 = 10. \times 10^{-6}\,\mathrm{K}^{-1}$. All the four layers have the same thickness, and it is equal to 1/4 of the total plate thickness. This particular plate configuration has been considered in order to create for the same plate, the BTDs for each multifield problem analyzed.

Firstly, few values of the stress and displacement components related to the plate considered are reported in Tab.s 7, 8, 9 and 10 for the mechanical, thermal and piezoelectric loads. The results are computed by means of the LD4 and ED4 models. It can be noted that, in general, the solutions offered by the LD4 and ED4 models are in good agreement when a thin plate is considered.

7.1 BTDs for the ESL scheme

Once the reference solutions are introduced, it is possible to define the BTDs for the multifield plate analysis. ESL approach is considered, and the BTDs for the ED4 model are reported in Fig.s 7 and 8 for the thin and thick geometry, respectively. These curves are defined considering the in-plane stress σ_{xx}. It can be noted that in general the reduced refined models for the piezoelectric case have a higher computational cost than the reduced models for the mechanical and thermal case, since the variables of the electric potential are retained. It can be noted that the models located on the BTDs for both the thermal and mechanical cases have the same accuracy when a thin plate is considered, while the BTDs for the piezoelectric case present a significant difference between the sensor and actuator configuration. The models of the BTD for the sensor configuration have better accuracy (lower error) than the actuator case. This fact holds for both the thick and thin plate cases. It can be observed that the models of the BTD for the mechanical case offers the best accuracy. Note that the reference solution is obtained with a LD4 model; for this reason, the minimum errors are always positive.

The representation of some of the reduced models which belong to the BTDs of Fig.s 7 and 8 are reported in Tab. 11 for the thin plate case and in Tab. 12 for the thick plate case, respectively. M/M_e indicates the number of the retained terms on the total number of terms in the reference model. It is possible to note that for a given number of terms and a stress component, the retained variables are different as a different type of load is considered. It should be mentioned that the reduced refined models for BTDs related to the the mechanical and thermal case present common active displacement variables for the particular problem considered (variables u_{x1}, u_{x2}, u_{x3}, u_{x4}, u_{y2} u_{z1} and u_{z2} are present in all models), while the reduced refined models for the piezoelectric case are quite different from the previous cases. In addition, the reduced refined models for the piezoelectric case are different as the sensor or actuator configuration is employed. The stress σ_{xx} distribution is evaluated by means of the reduced models of the BTDs for the thick plate case, and the result is reported in Fig. 9. It is possible to note that the solutions proposed are in good agreement with the reference solution.

An in-depth analysis of the difference between the BTDs for the sensor and actuator configurations is carried out, and the results are reported in Fig. 10. These BTDs are constructed considering the potential distribution Φ. The results show that the reduced models for the actuator configuration offer better accuracy than the reduced models for the sensor configuration. It should be mentioned that the accuracy of the BTDs related to the sensor configuration is very similar for both thin and thick plate geometry. On the contrary, the accuracy of the refined models related to the actuator plate configuration is higher in the case of the thin geometry than in the case of the thick geometry. The potential distributions computed by means of the reduced models which belong to the BTDs are depicted in Fig.s 11. In general, the reduced models make it possible to compute solutions that are in good agreement with the reference solution. In particular, it is possible to note that better accuracy is obtained for the actuator configuration. The results related to the ED4 models showed that

- the geometry and the type of load affect the process of selection of the terms;
- in general, the models located on the BTD for the mechanical load case offer the best accuracy while the lowest accuracy has been registered for the models of the BTD related to the piezoelectric

plate case (actuator configuration);

- in some cases, the reduced refined models for the mechanical and thermal stress analyses have in common several displacement variables.

7.2 BTDs for the LW scheme

The definition of BTDs is performed also for LD4 models, and the results are reported in Fig.s 12 and 13 for thin and thick plates, respectively. The stress σ_{xx} distribution is considered for the definition of these curves. It is possible to note that the reduced models which belong to the BTDs for the mechanical and thermal loads present approximately the same accuracy. The highest computational cost is registered for the BTDs related with the piezoelectric plate case since the potential distribution variables are included in the model. In particular, it can be noted that in the case of the thick plate piezoelectric plate, considering the actuator configuration, the highest error is equal to the 60%.

The representation of the models of these BTDs are reported in Tab. 13. It is possible to note that for the case herein considered, the reduced refined models which belong to the BTDs for the mechanical and thermal loads are different. The results reported show that the accuracy of the models related with the mechanical and thermal loads is higher than the accuracy of the models related with the piezoelectric case, given the same number of active terms (25). The stress distribution for the reduced models reported in Tab. 13 are depicted in Fig. 14. It is possible to note that the reduced models make it possible to compute the stress distribution in good agreement with the reference solution.

The influence on the selection of terms for the electric potential Φ is analyzed. The results are depicted in Fig. 15. As already noted for the ED4 model, the accuracy offered by the reduced model for the actuator configuration is higher than the accuracy offered by the reduced model for the sensor actuator. The lowest accuracy is obtained for the thick plate case in the sensor configuration, and it is equal to the 6%. The potential distributions computed with these reduced models are depicted in Fig. 16. It is possible to note that the accuracy of these models is particularly good. Differently from the ED4 models case, the potential distribution computed for the thick and thin plates in the sensor configuration present a better agreement with the reference solution than the ED4 models. The results showed that

- the type of load and geometry influences the retained terms of an LW model for a given number of active terms;
- in some cases, the configuration of a piezoelectric plate (sensor or actuator) may not affect the selection of terms.

8 Conclusion

A simply supported laminated plate was analyzed considering the effect of different types of loads. The Navier-like closed form solution was adopted, and the Carrera Unified Formulation was employed to generate the refined models. The axiomatic / asymptotic technique was used to detect the terms which are essential for the proper static response detection and, in this way, to create the Best Theory Diagram (BTD) for multifield plate analyses. The influence of the geometry was considered through the length-to-thickness (a/h) ratio and the BTDs were obtained considering the stress σ_{xx}, and in some cases the potential distribution Φ. The analyses showed that

1. the type of the load and the geometry influences to a great extent the selection of the relevant terms for both LW and ESL approaches; in addition, the type of load influences the number of the models for a given problem;
2. the accuracy of the LW models related to the mechanical and thermal load cases are very similar;
3. the accuracy of the models related to the piezoelectric case is influenced by the type of the configuration considered (actuator or sensor); in general, the models related to the actuator configuration are more accurate than the models for the sensor configuration.

Future works can be performed considering different boundary conditions (in this case the use of the finite element method is mandatory). In addition, shell geometries can be considered and the effect of a piezo-thermal load on the retained displacement variables can be analyzed.

Acknowledgments

This research received no specific grant from any funding agency in the public, commercial, or not-for-profit sectors.

References

Almansi E (1897) Use of the Stress Function in Thermoelasticity. *Memorie della Reale accademia delle scienze di Torino* 47(2).

A.N.S. Institute (1987) *Ieee standard on piezoelectricity*. Technical Report NASA CR 4665, IEEE, March 1987.

Argyris J and Tenek L (1997) Recent advances in computational thermostructural analysis of composite plates and shells with strong nonlinearities. *Applied Mechanics Reviews* 50(5):285-306.

Ballhause D, D'Ottavio M, Kroplin B and Carrera E (2005) A unified formulation to assess multilayered theories for piezoelectric plates. *Computer & Structures* 83:1217-1235.

Bhaskar K, Varadan TK and Ali JSM (1996) Thermoelastic solutions for orthotropic and anisotropic composite laminates. *Composites* 27(B):415-420.

Carrera E (1997) C_z^0 requirements - models for the two dimensional analysis of multilayered structures. *Composite Structures* 37(3-4):373-383.

Carrera E (2003) Theories and finite elements for multilayered plates and shells: A unified compact formulation with numerical assessment and benchmarking. *Archives of Computational Methods in Engineering* 10(3):215-296.

Carrera E (2002) Temperature profile influence on layered plates response considering classical and advanced theories. *AIAA Journal* 40(9):1885-1896.

Carrera E and Brischetto S (2008) Analysis of thickness locking in classical, refined and mixed multilayered plate theories. *Composite Structures* 82(4):549-562.

Carrera E and Brischetto S (2010) Coupled thermo-mechanical analysis of one-layered and multilayered plates. *Composites Structures* 92:1793-1812.

Carrera E and Miglioretti F (2012) Selection of appropriate multilayered plate theories by using a genetic like algorithm. *Composite Structures* 94(3):1175-1186.

Carrera E and Petrolo M (2010) Guidelines and recommendation to construct theories for metallic and composite plates. *AIAA Journal* 48(12):2852-2866.

Carrera E and Petrolo M (2011) On the effectiveness of higher-order terms in refined beam theories. *Journal of Applied Mechanics* 78:1-17.

Carrera E, Giunta G and Petrolo M (2010) B.H.V. Topping. In: Developments and Applications in Computational Structures Technology *A Modern and Compact Way to Formulate Classical and Advanced Beam Theories*. Stirlingshire, UK: Saxe-Coburg Publications, pp. 75-112.

Carrera E, Brischetto S and Nali P (2011) *Plates and Shells for Smart Structures Classical and Advanced Theories for Modeling and Analysis*. New Delhi: Wiley.

Carrera E, Giunta G and Petrolo M (2011) *Beam Structures, Classical and Advanced Theories*. New Delhi: Wiley.

Carrera E, Miglioretti F and Petrolo M (2011) Accuracy of refined finite elements for laminated plate analysis. *Composite Structures* 93(5):1311-1327.

Carrera E, Miglioretti F and Petrolo M (2011) Guidelines and recommendations on the use of higher order finite elements for bending analysis of plates. *International Journal for Computational Methods in Engineering Science and Mechanics* 12(6):303-324.

Carrera E, Miglioretti F and Petrolo M (2012) Computations and evaluations of higher-order theories for free vibration analysis of beams. *Journal of Sound and Vibration* 331:4269-4284.

Carrera E, Cinefra M, Petrolo M and Zappino E (2014) *Finite Element Analysis of Structures through Unified Formulation*. John Wiley & Sons.

Darwin CR (1859) *On the origin of species by means of natural selection, or the preservation of favored races in the struggle for life*. London: John Murray.

Duhamel JMC (1837) Second memoire sur les phenomenes thermomecaniques. *J. de l'Ecole Polytechnique* 15(25):1-57.

Fonseca M and Fleming P (1993) Genetic algorithm for multiobjective optimization: formulation, discussion and generalization. In: *Proceedings of the 5th International Conference on Genetic Algorithms*, pp. 416-423. San Francisco, CA, USA: Morgan Kaufmann Publishers Inc.

Fourier JBJ (1822) *Theorie analytique de la chaleur*. Paris: Firmin Didot.

Hetnarski RB and Eslami MR *Thermal Stresses - Advanced Theory and Applications*. Editors: Barber, J R, Klarbring, Anders, Vol. 158.

Heyliger P (1994) Static behavior of laminated elastic/piezoelectric plates. *AIAA Journal* 32(12):2481-2484.

Hildebrand FB, Reissner E and Thomas GB (1938) Notes in the foundations of the theory of small displacement of orthotropic shells. Technical report, NASA, March.

Kirchhoff G (1850) Uber das gleichgewicht und die bewegung einer elastischen scheibe. *Journal fur reins und angewandte Mathematik* 40, 51-88.

Lekhnitskii GS (1968) *Anisotropic Palates,* 2^{nd} *edition*. SW Tsai and Cheron, Bordon and Breach.

Love AEH (1927) *The Mathematical Theory of Elasticity*. Cambridge: Cambridge University Press.

Mashat DS, Carrera E, Zenkour AM and Al Khateeb SA (2013) Axiomatic/asymptotic evaluation of multilayered plate theories by using single and multi-points error criteria. *Composite Structures* 106:393-406.

Mashat DS, Carrera E, Zenkour AM and Al Khateeb SA (2014) Use of axiomatic/asymptotic approach to evaluate various refined theories for sandwich shells. *Compsosite Structures* 109:139-149.

Mindlin RD (1951) Influence of rotatory inertia and shear in flexural motions of isotropic elastic plates. *Journal of Applied Mechanics* 18:1031-1036.

Mindlin R (1972) High frequency vibrations of piezoelectric crystal plates. *International Journal of Solids and Structures* 8:895-906.

Mitchell J and Reddy JN (1995) A refined hybrid plate theory for composite laminates with piezoelectric laminae. *International Journal of Solids and Structures* 32(16):2345-67.

Murakami H (1993) Assessment of plate theories for treating the thermomechanical response of layered plates. *Composites Engineering* 3(2):137-149.

Navier CLMH (1827) Memoire sur les lois de l'equilibre et du movement des corps solides elastiques. *MÃ©moires de l'AcadÃ©mie des sciences, Paris* 7:375-393.

Neumann F (1855) *Vorlesung uber die Theorie des Elasticitat der festen Korper und des Lichtathers*. Leipzig: Teubner.

Noor AK and Burton WS (1992) Computational models for high-temperature multilayered composite plates and shells. *Applied Mechanics Reviews* 12(10):419-446.

Pagano JN (1969) Exact solutions for rectangular bidirectional composites and sandwich plate. *Journal of Composites Material* 4:20-34.

Pagano NJ (1970) Exact solutions for rectangular bidirectional composites and sandwich plate. *Journal of Composites Material* 4:20-34.

Pagano NJ and Hatfield SJ (1972) Elastic Behavior of Multilayered Bidirectional Composites. *AIAA Journal* 10(7):931-933.

Petrolo M and Lamberti A (2016) Axiomatic/asymptotic analysis of refined layer-wise theories for composite and sandwich plates. *Mechanics of Advanced Materials and Structures* 23(1):28-42.

Reddy JN (1997) *Mechanics of Laminated Plates, Theory and Analysis*. Boca Raton: CRC Press.

Reissner E (1945) The effect of transverse shear deformation on the bending of elastic plates. *Journal of Applied Mechanics* 12:69-76.

Tauchert TR (1991) Thermally induced flexure, buckling, and vibration of plates. *Applied Mechanics Reviews* 44(8):347-360.

Tedone O (1906) Allgemeine Theoreme der matematischen Elastizitatslehre (Integrationstheorie). *Encyklopadie der matematischen Wissenschaften* 4(D):55-214.

Tiersten HF (1969) *Linear Piezoelectric Plate Vibrations*. Plenum Press.

Vlasov BF (1957) On the equations of bending of plates. *Doklady Akademii Nauk Azerbaidzhanskoi SSR* 3:955-979.

Voigt W (1910) *Lehrbuch der Kristallphysik*. Berlin: Teubner.

Yang J and Yu J (1993) Equations for a laminated piezoelectric plate. *Archives of Mechanics* 45:653-664.

Tables

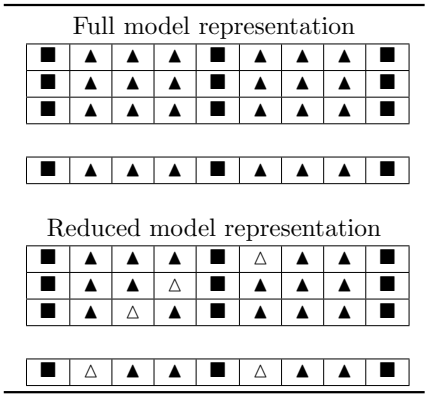

Table 1: Schematic representation of the displacement and potential field in a 2-layer plate for a full LD4 model (up) and an example of reduced model in which the terms u^2_{x2}, u^1_{y4}, u^1_{z3}, Φ^1_1, Φ^2_1 are deactivated (down).

Active term	Inactive term	Non-deactivable term
▲ ●	△ ○	■

Table 2: Symbols that indicate the status of a term in the expansion of variables.

					$a/h = 100$			
					3-layers laminate			
	$\overline{\sigma}_{xx}(z=\pm h/2)$		$\overline{\sigma}_{yy}(z=\pm h/6)$		$\overline{\sigma}_{xz}(z=0)$	$\overline{\sigma}_{yz}(z=0)$	$\overline{\sigma}_{xy}(z=\pm h/2)$	
Ref. (Pagano, 1969)	± 0.539		0.181		0.395	0.0828	∓ 0.0213	
LD4	± 0.539		0.181		0.395	0.0828	∓ 0.0214	
					5-layers laminate			
	$\overline{\sigma}_{xx}(z=\pm h/2)$		$\overline{\sigma}_{yy}(z=\pm h/3)$		$\overline{\sigma}_{xz}(z=0)$	$\overline{\sigma}_{yz}(z=0)$	$\overline{u}_z(z=0)$	
Ref. (Pagano and Hatfield, 1972)	± 0.539		± 0.360		0.272	0.205	1.006	
LD4	± 0.539		± 0.360		0.272	0.206	1.006	
					$a/h = 4$			
					3-layers laminate			
	$\overline{\sigma}_{xx}(z=\pm h/2)$		$\overline{\sigma}_{yy}(z=\pm h/6)$		$\overline{\sigma}_{xz}(z=0)$	$\overline{\sigma}_{yz}(z=0)$	$\overline{\sigma}_{xy}(z=\pm h/2)$	
Ref. (Pagano, 1969)	0.801	-0.755	0.534	-0.556	0.256	0.2172	-0.0511	0.0505
LD4	0.801	-0.755	0.534	-0.556	0.256	0.2180	-0.0511	0.0505
					5-layers laminate			
	$\overline{\sigma}_{xx}(z=\pm h/2)$		$\overline{\sigma}_{yy}(z=\pm h/3)$		$\overline{\sigma}_{xz}(z=0)$	$\overline{\sigma}_{yz}(z=0)$	$\overline{u}_z(z=0)$	
Ref. (Pagano and Hatfield, 1972)	0.685	-0.651	0.633	-0.626	0.238	0.229	4.291	
LD4	0.685	-0.651	0.634	-0.626	0.238	0.229	4.291	

Table 3: Assessment of LD4 model in the mechanical case. Stresses and displacement for a 3-layers ($0°/90°/0°$) and a 5-layers ($0°/90°/0°/90°/0°$) simply supported plate under bi-sinusoidal load for different thickness ratios. $\overline{u}_z = \frac{u_z \, 100 \, E_T \, h^3}{p_z \, a^4}$, $\overline{\sigma}_{xx/yy/xy} = \frac{\sigma_{xx/yy/xy}}{p_z \, (a/h)^2}$, $\overline{\sigma}_{xz/yz} = \frac{\sigma_{xz/yz}}{p_z \, (a/h)}$

	Cylindrical thermal load			
	$\overline{u}_x(z=\mp h/2)$	$\overline{u}_z(z=\mp h/2)$	$\overline{\sigma}_{xx}(z=\mp h/6)$	$\overline{\sigma}_{xz}(z=\mp h/6)$
		$a/h=100$		
Ref. (Bhaskar et al., 1996)	$\pm$4.449	2.855	$\pm$371.4	0.2987
LD4	$\pm$4.449	2.855	$\pm$371.4	0.2987
		$a/h=4$		
Ref. (Bhaskar et al., 1996)	$\pm$7.470	18.32	$\pm$372.3	2.830
LD4	$\pm$7.470	18.32	$\pm$372.3	2.806
	Bisinusoidal thermal load			
	$\overline{u}_x(z=\mp h/2)$	$\overline{u}_z(z=\mp h/2)$	$\overline{\sigma}_{xx}(z=\pm h/2)$	$\overline{\sigma}_{xz}(z=\mp h/6)$
		$a/h=100$		
Ref. (Bhaskar et al., 1996)	$\pm$16.00	10.26	$\pm$965.4	7.073
LD4	$\pm$16.00	10.26	$\pm$965.4	7.073
		$a/h=4$		
Ref. (Bhaskar et al., 1996)	$\pm$18.11	42.69	$\pm$1183	84.81
LD4	$\pm$18.11	42.69	$\pm$1183.2	84.81

Table 4: Assessment of LD4 model in the thermal case. Stresses and displacement for a 3-layers ($0°/90°/0°$) plate under thermal bi-sinusoidal load for different thickness ratios. Temperature values at the top and bottom of the plate are $t_{top}=1.0$, $t_{bot}=-1.0$. Reference temperature is $\bar{t}_0=1.0$. $\overline{u}_x=\frac{u_x}{h\,\alpha_L\,\bar{t}_0\,(a/h)}$, $\overline{u}_z=\frac{u_z}{h\,\alpha_L\,\bar{t}_0\,(a/h)^2}$, $\overline{\sigma}_{ij}=\frac{\sigma_{ij}}{E_T\,\alpha_L\,\bar{t}_0}$

z	$u_x\times10^{12},[m]$		Φ, [V]		$\sigma_{zz}\times10,[Pa]$		$\tilde{D}_z\times10^{13},[C/m^2]$	
	3D	LD4	3D	LD4, $\times10^1$	3D	LD4	3D	LD4
0.500	-47.549	-47.552	0.0000	0.0000	10.000	10.000	160.58	160.58
0.400	-23.732	-23.733	0.0598	0.0599	9.5151	9.5153	-0.3382	-0.3348
0.000	20.392	20.394	0.0611	0.0611	4.9831	4.9855	0.5052	0.5053
-0.400	39.309	39.313	0.0756	0.0756	0.4868	0.4867	1.4587	1.4590
-0.500	60.678	60.682	0.0000	0.0000	0.0000	0.0000	-142.46	-142.46

Table 5: Assessment of LD4 model in the case of piezo-mechanic static response of a ($90°/0°$) plate with external piezoelectric layers. Comparison with 3D analytical solution from Heyliger (1994) - $a/h=4$ - Sensor configuration.

z	$u_x\times10^{12},[m]$		$\Phi,[V]$		$\sigma_{zz}\times10^3,[Pa]$		$\sigma_{xz}\times10^3,[Pa]$	
	3D	LD4	3D	LD4	3D	LD4	3D	LD4
0.500	-32.764	-32.765	1.0000	1.0000	0.0000	0.0000	0.0000	0.0000
0.400	4.7356	4.7352	0.9929	0.9931	-7.5482	-7.5339	56.259	56.034
0.000	0.0295	0.0297	0.4476	0.4477	-14.612	-14.629	-23.866	-23.863
-0.400	-1.7839	-1.7834	-0.0010	-0.0010	-1.8733	-1.8958	-23.379	-23.376
-0.500	-2.8625	-2.8618	0.0000	0.0000	0.0000	0.0000	0.0000	0.0000

Table 6: Assessment of LD4 model in the case of piezo-mechanic static response of a ($90°/0°$) plate with external piezoelectric layers. Comparison with 3D analytical solution from Heyliger (1994) - $a/h=4$ - Actuator configuration.

	$a/h=100$		$a/h=4$		$a/h=100$		$a/h=4$	
	LD4				ED4			
z	$\overline{u}_z$	$\overline{\sigma}_{xx}$	$\overline{u}_z$	$\overline{\sigma}_{xx}$	$\overline{u}_z$	$\overline{\sigma}_{xx}$	$\overline{u}_z$	$\overline{\sigma}_{xx}$
-0.5	0.3963	-0.2328	0.9744	-0.2881	0.3957	-0.2304	0.7917	-0.3116
-0.4	0.3963	-0.1888	0.9915	-0.1828	0.3957	-0.1895	0.8063	-0.1705
0.0	0.3964	-0.0017	1.0336	0.0100	0.3958	-0.0019	0.8481	-0.0398
0.4	0.3963	0.1629	1.0782	0.2080	0.3957	0.1635	0.8653	0.1964
0.5	0.3963	0.2069	1.0662	0.3230	0.3957	0.2043	0.8538	0.3408

Table 7: LD4 and ED4 reference solutions in terms of transversal displacement and in-plane stress. Mechanic static response of a ($90°/0°$) plate with external piezoelectric layers for different thickness ratios.

	$a/h = 100$		$a/h = 4$		$a/h = 100$		$a/h = 4$	
	LD4				ED4			
z	$\overline{u}_z$	$\overline{\sigma}_{xx}$	$\overline{u}_z$	$\overline{\sigma}_{xx}$	$\overline{u}_z$	$\overline{\sigma}_{xx}$	$\overline{u}_z$	$\overline{\sigma}_{xx}$
-0.5	0.4927	136.0200	0.5636	133.5900	0.4894	130.6500	0.5426	132.5100
-0.4	0.4927	102.8600	0.5445	99.8270	0.4894	104.6700	0.5238	104.1500
0.0	0.4926	-4.0093	0.4742	-3.4198	0.4893	-4.0312	0.4814	-3.7648
0.4	0.4927	-162.5700	0.5445	-159.3700	0.4894	-158.1200	0.5238	-157.4100
0.5	0.4927	-195.7300	0.5636	-190.3900	0.4894	-183.7100	0.5426	-184.8000

Table 8: LD4 and ED4 reference solutions in terms of transversal displacement and in-plane stress. Thermal static response of a (90°/0°) plate with external piezoelectric layers for different thickness ratios.

	$a/h = 100$		$a/h = 4$	
z	$\sigma_{xx} \times 10^4, [Pa]$	$\Phi, [V/m]$	$\sigma_{xx} \times 10^{-4}, [Pa]$	$\Phi, [V/m]$
	LD4			
-0.5	-0.24970	0.0000	-5.2226	0.00000
-0.4	-0.20186	3.0819	-3.2037	0.00646
0.0	-0.00147	6.4150	0.1701	0.00865
0.4	0.17977	3.0802	3.5513	0.00519
0.5	0.22761	0.0000	5.7604	0.00000
	ED4			
-0.5	-0.24934	0.0000	-5.4224	0.00000
-0.4	-0.20200	3.0830	-3.1613	0.00609
0.0	-0.00166	6.4088	0.0827	0.00953
0.4	0.17985	3.0821	3.2304	0.00538
0.5	0.22710	0.0000	4.6103	0.00000

Table 9: LD4 and ED4 reference solutions in terms of in-plane stress and electric potential. Piezo-mechanic static response of a (90°/0°) plate with external piezoelectric layers for different thickness ratios. Sensor configuration.

	$a/h = 100$		$a/h = 4$	
z	$\sigma_{xx}, [Pa]$	$\Phi, [V/m]$	$\sigma_{xx}, [Pa]$	$\Phi, [V/m]$
	LD4			
-0.5	-0.02659	0.00000	1.04780	0.00000
-0.4	-0.02736	0.00035	0.53439	-0.00091
0.0	0.00246	0.49993	-0.09214	0.45799
0.4	-0.02859	0.99961	-0.08477	0.97355
0.5	-0.02604	0.00000	1.33300	0.10000
	ED4			
-0.5	-0.03304	0.00000	2.06260	0.00000
-0.4	-0.02559	0.00034	1.05410	-0.00179
0.0	0.00013	0.49993	-0.20510	0.45939
0.4	-0.02780	0.99961	-0.01939	0.97425
0.5	-0.03504	0.10000	1.06870	1.00000

Table 10: LD4 and ED4 reference solutions in terms of in-plane stress and electric potential. Piezo-mechanic static response of a (90°/0°) plate with external piezoelectric layers for different thickness ratios. Actuator configuration.

	Mechanical load $M/M_e = 9/15$	Thermal load $M/M_e = 9/15$
	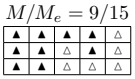	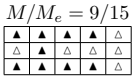
Error	1.0498 %	0.0120%
	Piezoelectric load	
	Sensor $M/M_e = 10/32$	Actuator $M/M_e = 10/32$
	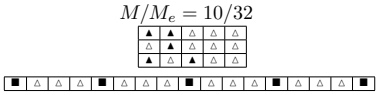	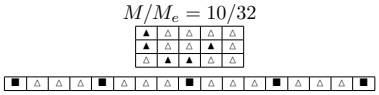
Error	1.9703 %	7.6621 %

Table 11: Reduced ED4 models for a $(90°/0°)$ plate with external piezoelectric layers - Multifield analyses. Thin case, $a/h = 100$.

	Mechanical load $M/M_e = 10/15$	Thermal load $M/M_e = 10/15$
	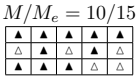	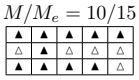
Error	2.9268 %	4.8339%
	Piezoelectric load	
	Sensor $M/M_e = 10/32$	Actuator $M/M_e = 10/32$
	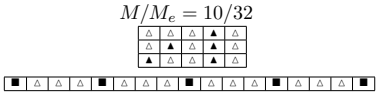	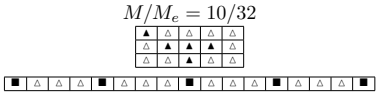
Error	4.5933 %	16.3465 %

Table 12: Reduced ED4 models for a $(90°/0°)$ plate with external piezoelectric layers - Multifield analyses. Thick case, $a/h = 4$.

	Mechanical load $M/M_e = 25/51$	Thermal load $M/M_e = 25/51$
		
Error	7.6734×10^{-2} %	5.1093×10^{-2} %
	Piezoelectric load	
	Sensor $M/M_e = 25/68$	Actuator $M/M_e = 25/68$
		
Error	0.2847 %	0.5683 %

Table 13: Reduced LD4 models for a $(90°/0°)$ plate with external piezoelectric layers - Multifield analyses. Thick case, $a/h = 4$.

Figures

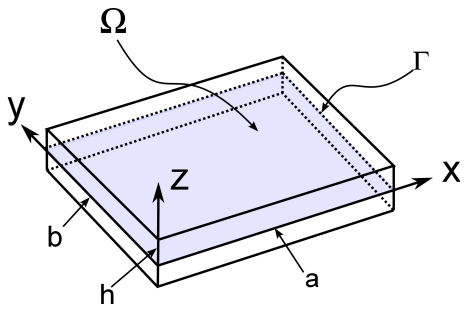

Figure 1: Plate geometry and notation.

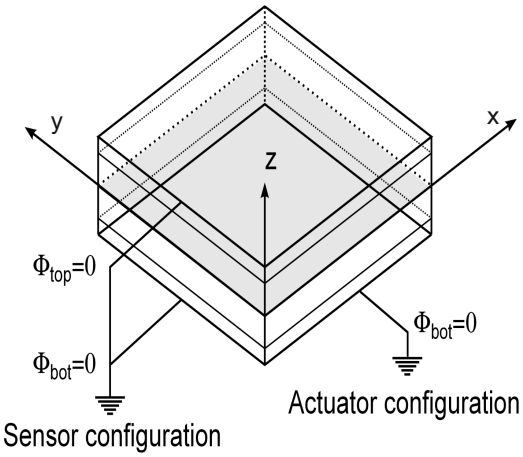

Figure 2: Piezoelectric plate.

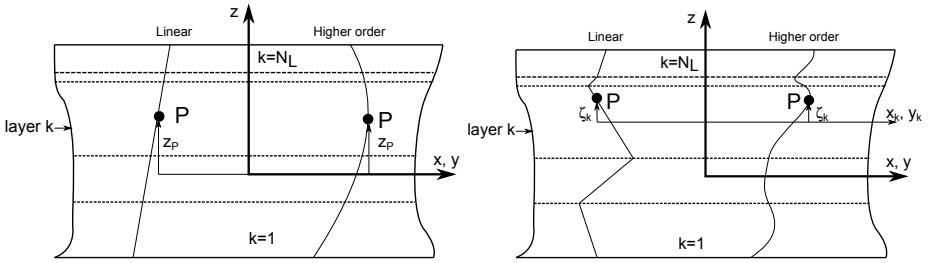

(a) Equivalent Single Layer scheme (b) Layer Wise scheme

Figure 3: Linear and higher-order ESL and LW examples.

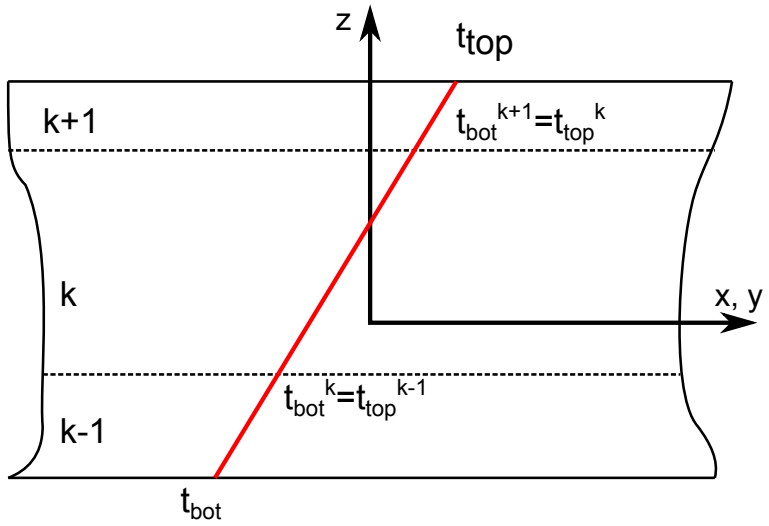

Figure 4: Temperature distribution.

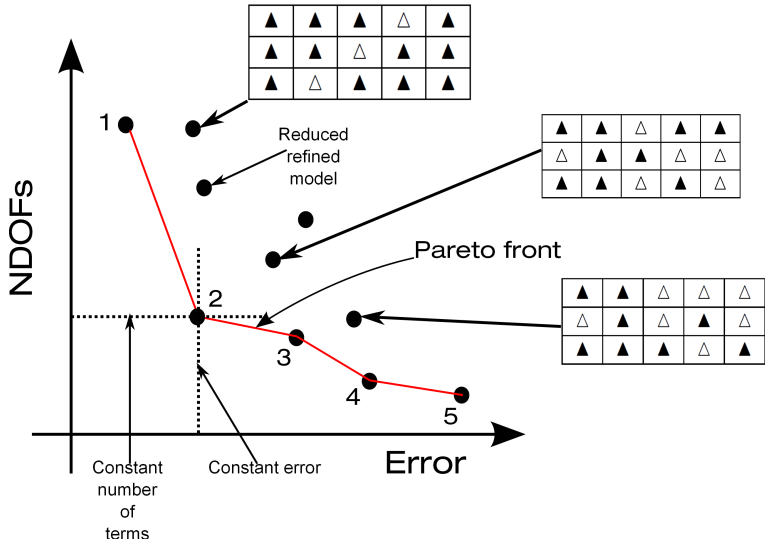

Figure 5: Example of representation of reduced refined models in the Best Theory Diagram.

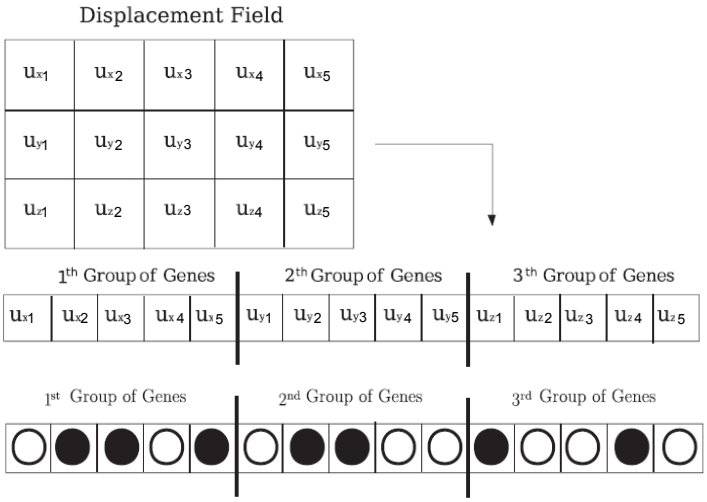

Figure 6: Displacement variables of a refined model and genes of an individual. Full black circles indicate active terms and empty circles deactivated ones.

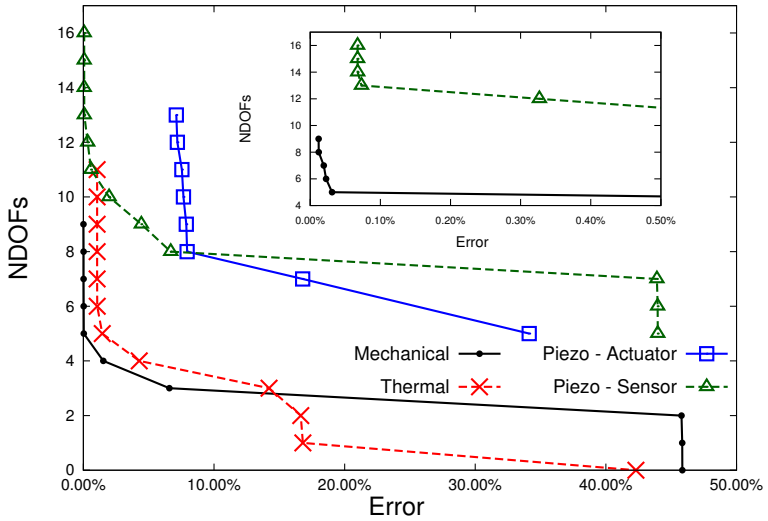

Figure 7: BTDs for ED4 model - mechanical, thermal and piezoelectric load cases, $a/h = 100$ - stress σ_{xx}. Lower errors are considered in the smaller picture.

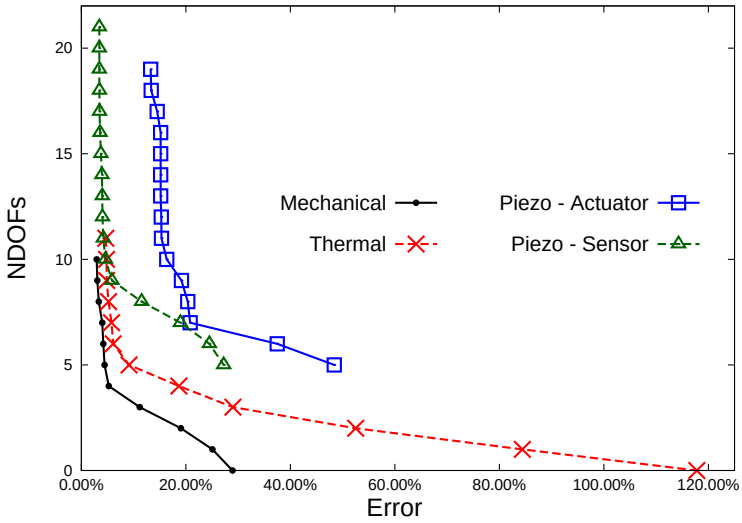

Figure 8: BTDs for ED4 model - mechanical, thermal and piezoelectric load cases, $a/h = 4$ - stress σ_{xx}.

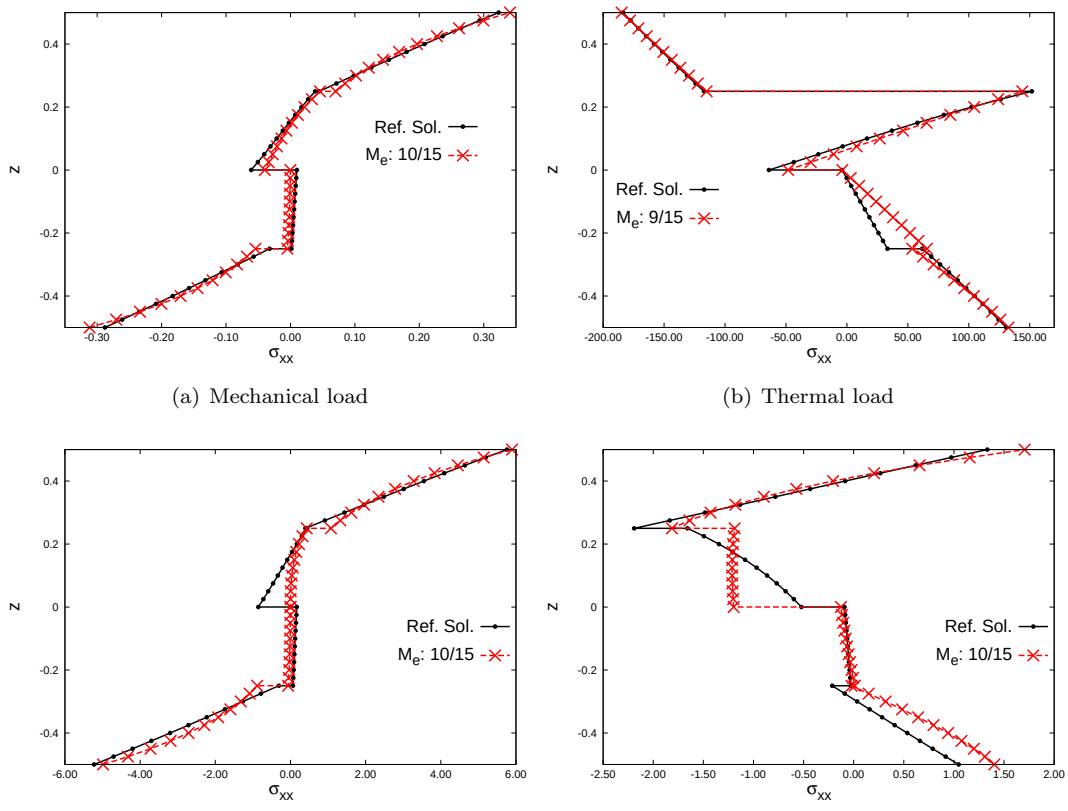

(a) Mechanical load

(b) Thermal load

(c) Piezoelectric load - sensor

(d) Piezoelectric load - actuator

Figure 9: Stress σ_{xx} distribution along the thickness. ED4 model, $a/h = 4$.

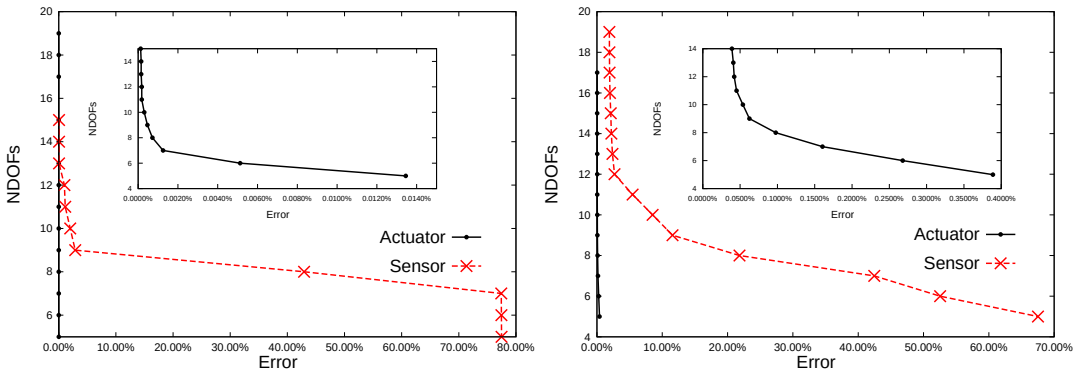

(a) $a/h = 100$ (b) $a/h = 4$

Figure 10: BTD for ED4 model - piezoelectric load case, Φ. Lower errors are considered in the smaller pictures.

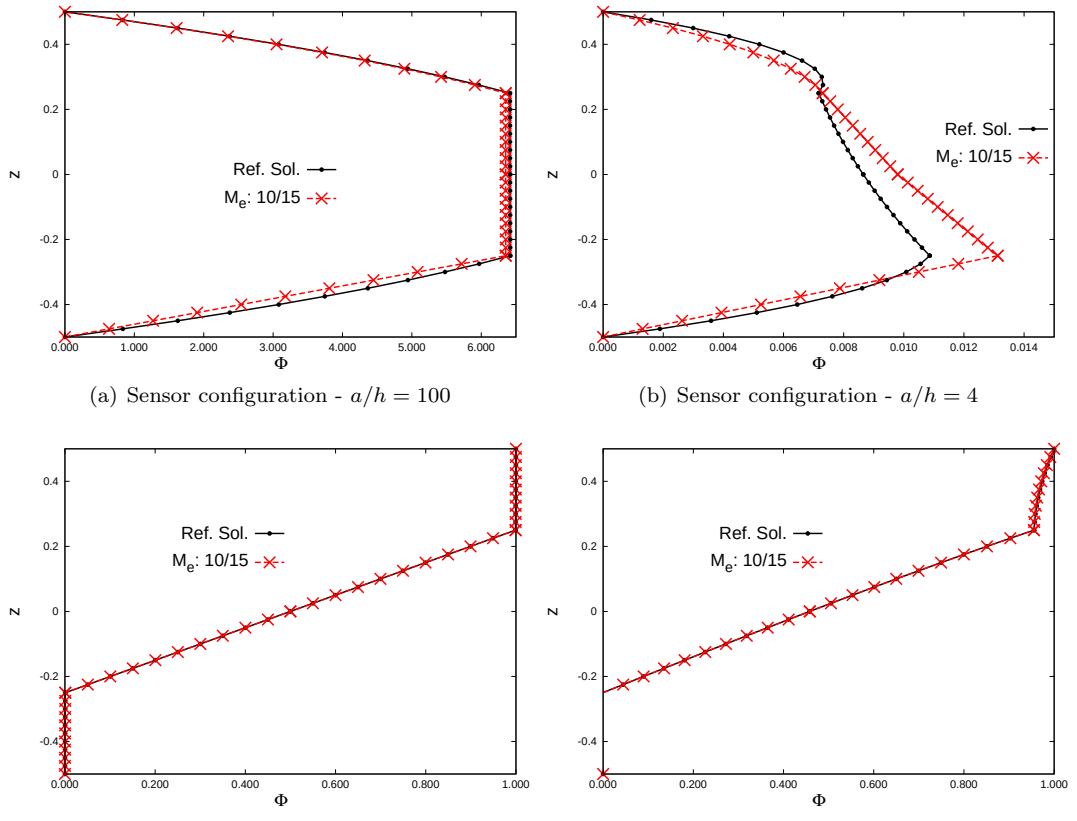

(a) Sensor configuration - $a/h = 100$ (b) Sensor configuration - $a/h = 4$

(c) Actuator configuration - $a/h = 100$ (d) Actuator configuration - $a/h = 4$

Figure 11: Potential Φ distribution along the thickness. ED4 model.

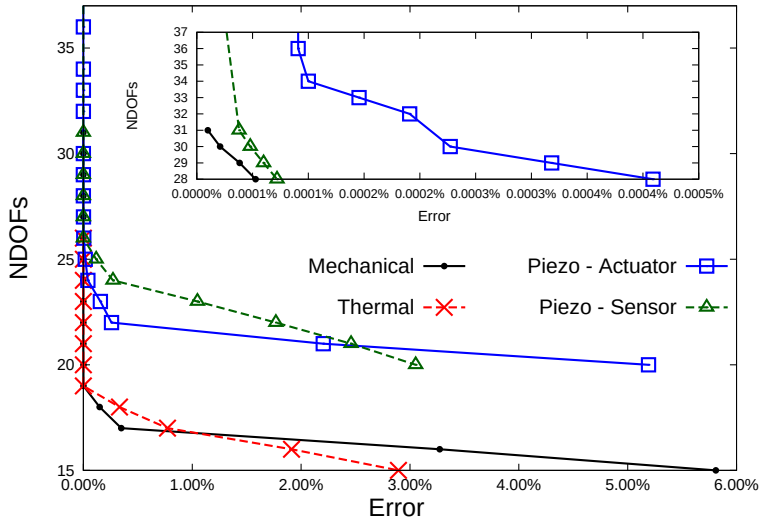

Figure 12: BTDs for LD4 model - mechanical, thermal and piezoelectric load cases, $a/h = 100$ - stress σ_{xx}. Lower errors are considered in the smaller picture.

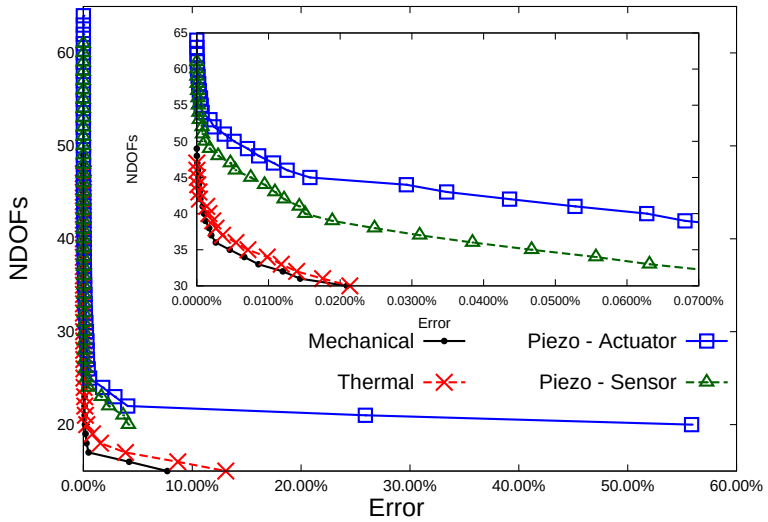

Figure 13: BTDs for LD4 model - mechanical, thermal and piezoelectric load cases, $a/h = 4$ - stress σ_{xx}. Lower errors are considered in the smaller picture.

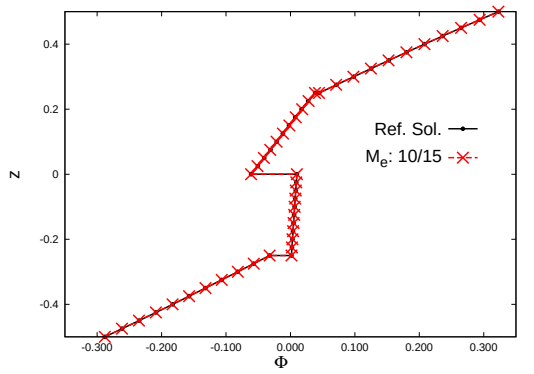

(a) Mechanical load

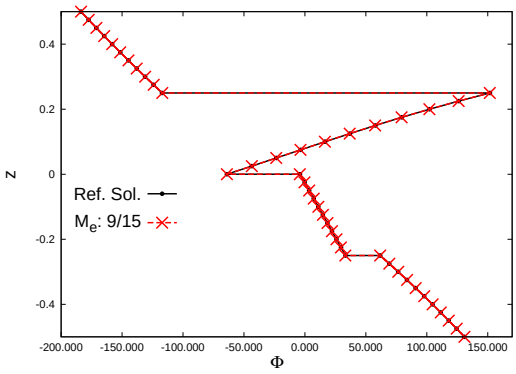

(b) Thermal load

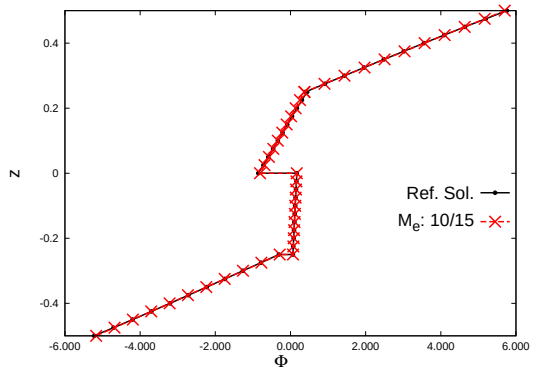

(c) Piezoelectric load - sensor

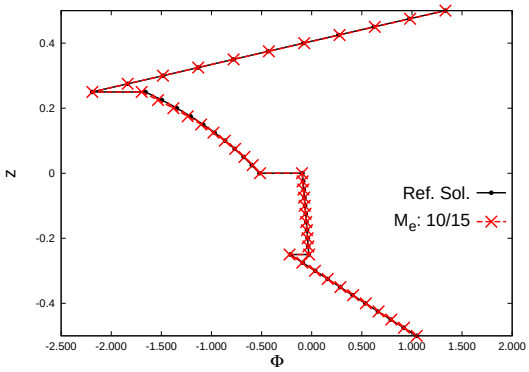

(d) Piezoelectric load - actuator

Figure 14: Stress σ_{xx} distribution along the thickness. LD4 model, $a/h = 4$.

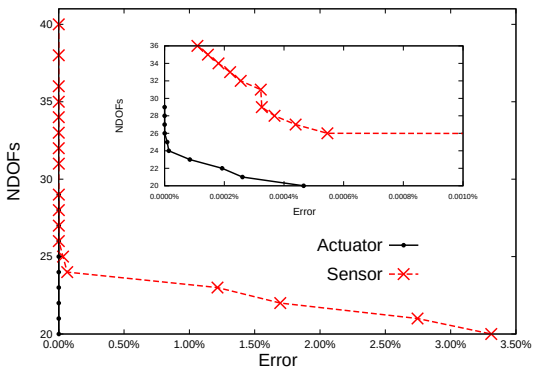

(a) $a/h = 100$

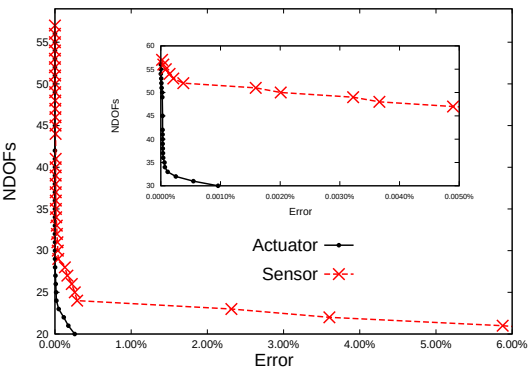

(b) $a/h = 4$

Figure 15: BTD for LD4 model - piezoelectric load case, Φ. Lower errors are considered in the smaller pictures.

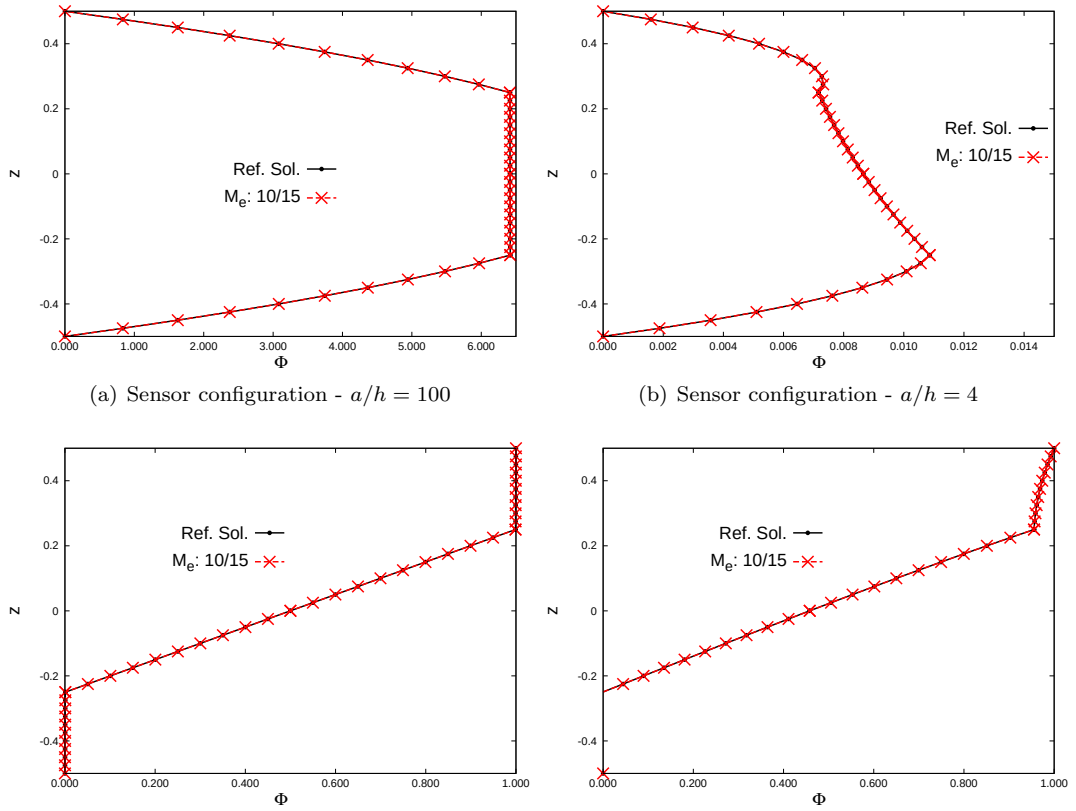

(a) Sensor configuration - $a/h = 100$

(b) Sensor configuration - $a/h = 4$

(c) Actuator configuration - $a/h = 100$

(d) Actuator configuration - $a/h = 4$

Figure 16: Potential Φ distribution along the thickness for LD4 model.